Atmos. Chem. Phys. Discuss.,
https://doi.org/10.5194/acp-2017-280-AC1, 2017

Atmospheric Chemistry and Physics Discussions

Interactive comment on "Improved rain-rate and drop-size retrievals from airborne and spaceborne Doppler radar" *by* Shannon L. Mason et al.

Shannon L. Mason et al.

s.l.mason@reading.ac.uk

Received and published: 6 July 2017

We thank the reviewers for their constructive comments, and hope that our responses have helped to improve the paper.

A common thread across the reviews was a request for more justification of the retrieval of a height-invariant Nw, and for evaluation of the retrievals through the vertical profile. In response we have added Figs. 5, 9 & 12 evaluating the averaged vertical profile of retrieved and forward-modelled variables in key precipitation regimes: moderate stratiform rain (case 1), light stratiform rain with strong evaporation (case 2), and moderate warm rain (case 3).

In evaluating the instances where the constant-Nw representation was not able to re-

produce the profile of 9.6 GHz radar observations, we thought it worthwhile to add a demonstration of the retrieval in which Nw is represented as a linear gradient (Section 6). We show that introducing another degree of freedom allows us to resolve some of the variations in the DSD through the profile as expected for collision-coalescence, and that these changes lead to an improved ability to forward-model the independent 9.6 GHz radar measurements. This is possible with the high vertical resolution of the airborne radar observations, and therefore worth demonstrating, but we do not necessarily anticipate retrieving a vertical profile of Nw from EarthCARE, which will have coarser 500m vertical resolution.

Major comments

1. I wonder how the absorption by liquid water clouds is handled. Liquid phase clouds below the melting layer will contribute to the total PIA. Their contribution can be substantial especially for lighter rainfall. Neglecting cloud absorption will result in overestimation of PIA due to rain. Cloud base heights can be significantly lower than the melting layer.

Radar attenuation by liquid cloud water is estimated within the forward model as for liquid rain water; however the detection of liquid clouds below the melting layer is difficult from above, where lidar tends to be extinguished and radar is dominated by the larger drops. We can be confident that the rain will dominate the radar attenuation, but it's true that this will be an upper estimate of the attenuation attributed to rain, and could include some fraction due to unseen clouds.

Changes:

This uncertainty has been made more explicit in Section 2.2 Target Classification; the relevant paragraph now includes an additional statement:

> As a result of the uncertain presence of liquid clouds within rainy profiles, the path-integrated attenuation of the radar that is attributed to rain may be partially due to undiagnosed liquid cloud.

2. Assuming that Nw is constant with height does not account for drop collision-coalescence, evaporation and breakup processes. It is a rather heavy assumption and it needs more justification.

Retrieving constant Nw for each profile is an improvement over assuming Nw is constant everywhere; however, we agree that the representation of Nw is not expected to be borne out physically in many cases. Therefore the constant Nw may be best interpreted as a profile-averaged Nw; but this warrants further discussion in the text.

There may indeed be sufficient information in some cases to retrieve more complex representations of the profile of Nw, may better fit our understanding of microphysical processes, and we agree this was important to discuss in more detail.

Changes:

To better justify the decision to retrieve constant Nw, we have added the following discussion in Section 2.3.3 defining the rain state variables:

> Additional state variables increase the degrees of freedom of the retrieval, and require more information from observational variables to constrain the

> retrieval. Therefore we retrieve a single value of Nw for each profile, with the physical interpretation of representing Nw as constant with height, or as the vertically-averaged value. The representation of Nw as constant with height is not expected to be borne out in cases where evaporation or collision-coalescence processes modify the drop number concentration through the vertical profile.

To explore the possibility of retrieving more detailed profiles of Nw, we have added Section 6, in which we retrieve Nw as a linear gradient for the warm rain case. The vertical profile of moderate warm rain is evaluated against the 9.6-GHz radar variables, and we show that by allowing the additional degree of freedom for a linear gradient of Nw we can better represent the mean Doppler velocity toward the surface, improving the fit to independent radar measurements, as well as (qualitatively) resolving the drop growth, and decreasing drop concentration, toward the surface we would expect from collision-coalescence processes in this context.

In the discussion and conclusions, we have added a paragraph to discuss the representation of Nw, summarising the findings of Section 6.

Other comments

1. Do you account for changes in raindrop terminal velocities with altitude as air density changes?

Terminal velocity is corrected for air density through the profile, however this had been unclear in the methods section (“. . . corrected for air density”).

Changes:

The description of mean Doppler velocity now says "...scaled to account for air density changes with altitude."

2. From the text I understood that gaseous attenuation is calculated from model profiles of temperature and humidity. In stratiform rain, however, relative humidity is often 90-95% and if model profiles suggest lower humidity (e.g., the model does not forecast rain in a particular pixel) the water vapor absorption contribution in PIA can be underestimated.

Yes, the relative humidity profile from the model is not updated in the presence of rain. In practice for the cases studied here, we have confirmed that the relative humidity in the model data already exceeds 90% for most of the rainy part of the vertical profile.

However the situation seems likely to occur at times, so the water vapour contribution to gaseous attenuation could be set in the algorithm to be the larger of the re-analysis and 90%.

3. The statement that the gradient method requires an assumption of constant rain rate with height is misleading. In fact it requires an assumption that non-attenuated reflectivity changes are small compared to changes due to attenuation. This method provides an average rain rate in the height interval which is used to calculate the gradient.

Thank you for this clarification.

Changes:

The text now reads:

> Both approaches are implemented simultaneously, so that whereas the gradient method of Matrosov et al. (2007) is applied only at moderate to heavy rain rates wherein it can be assumed that the gradient of apparent radar reflectivity is dominated by attenuation, within the CAPTIVATE variational scheme the gradient of R and k can be estimated simultaneously from the profile of radar reflectivity and PIA.

4. When using 9.6 GHz data, do you account for rain attenuation at this frequency? Estimates show that attenuation at X-band at 10 mm/h at nadir pointing and in a 4 km thick layer could be around 1.3 dB. In addition to that the melting layer attenuation will add a contribution, which cannot be neglected.

The attenuation of the 9.6 GHz radar due to both rain and the melting layer are included in the forward model.

Changes:

In Section 2.3.4 on the melting layer, the corresponding value of k for X-band radar from Matrosov (2008) are now given.

In Section 2.3.5 on the radar forward model, we now mention both frequencies explicitly.

5. How well are radar beams at X and W bands matched? The DDV measurements are very sensitive to beam mismatches.

The X- and W-band radars aboard ER-2 have been previously used for DDV measurements (e.g. Tian et al. 2007) from CRYSTAL-FACE, and by averaging to 5-second (1 km) along-track we expect that the matching between the two radar sampling volumes is strongly correlated despite differences in beam widths.

In terms of pointing error, visually there is no appearance of significant features being poorly correlated, and we do not correct for any known differences in radar pointing.

6. I believe the reference to Matrosov et al. (2008) in JAS in line 10 on page 7 for eq. (6) is wrong, it should be the reference to Matrosov (2008) IEEE TGARS, 1039-1047, doi: 10.1109/TGRS.2008.915757 This equation provides two-way attenuation. Your assumption of Xm=1 km actually corresponds to the melting layer thickness of 0.5 km, which accidentally is about right as melting layers often have thicknesses of around 0.5 km. Please correct the reference and the Xm definition.

Thank you for catching this: this was indeed the paper we intended.

Changes:

We have corrected the reference.

The definition of Xm is updated.

7. Figure 3. It appears that PIA is saturated at values lower than 60 dB, but the text says it is 65 dB.

Fixed.

8. Did you estimate what is the uncertainty of using the Mie theory instead of calculations for oblate raindrops?

The T-matrix method is also implemented in CAPTIVATE, so we calculated the effect of including oblate drops at larger diameters. Using Thurai et al. (2007) and Zhang et al. (2001) for the axial ratios of raindrops, the error in total backscatter due to assuming spherical drops is around 5% for a DSD with D0 of 1.5mm, which is roughly the largest D0 retrieved in this study; and much less for smaller median drop diameters. Errors in extinction are less than 2%.

Changes:

These uncertainties are now noted in Section 2.3.5 when radar reflectivity and extinction are described.

9. Figure 4 shows PIA-based retrievals also for the period when the W-band signal was completely extinguished (between 16:02 and 16:03 UTC), so PIA was not available. How it is possible?

When the radar is fully attenuated and the surface backscatter signal is indistinguishable from the noise, the PIA signal saturates, but is still available. This effect is accounted for in the forward-model, so that while the saturated PIA no longer provides an accurate estimate of the total attenuation in the profile, the information that the radar is extinguished still provides some information for the retrieval.

Editorial comments

1. Since you use natural logarithms in (4), (5), (9) and Table 1, you should change "log" to "ln".

Fixed

2. Page 8 line 24 and Table 2: 3 dBZ -> 3 dB (relative units).

Fixed.

3. Table 2. You do not measure Z as it is given in (7), but rather you measure attenuated Z.

True. The apparent reflectivity Za is now introduced in this section, and used in Table 2.

Interactive comment on Atmos. Chem. Phys. Discuss., https://doi.org/10.5194/acp-2017-280, 2017.

Atmos. Chem. Phys. Discuss.,
https://doi.org/10.5194/acp-2017-280-AC2, 2017

Atmospheric Chemistry and Physics Discussions

Interactive comment on "Improved rain-rate and drop-size retrievals from airborne and spaceborne Doppler radar" *by* Shannon L. Mason et al.

Shannon L. Mason et al.

s.l.mason@reading.ac.uk

Received and published: 6 July 2017

We thank the reviewers for their constructive comments, and hope that our responses have helped to improve the paper.

A common thread across the reviews was a request for more justification of the retrieval of a height-invariant Nw, and for evaluation of the retrievals through the vertical profile. In response we have added Figs. 5, 9 & 12 evaluating the averaged vertical profile of retrieved and forward-modelled variables in key precipitation regimes: moderate stratiform rain (case 1), light stratiform rain with strong evaporation (case 2), and moderate warm rain (case 3).

In evaluating the instances where the constant-Nw representation was not able to re-

produce the profile of 9.6 GHz radar observations, we thought it worthwhile to add a demonstration of the retrieval in which Nw is represented as a linear gradient (Section 6). We show that introducing another degree of freedom allows us to resolve some of the variations in the DSD through the profile as expected for collision-coalescence, and that these changes lead to an improved ability to forward-model the independent 9.6 GHz radar measurements. This is possible with the high vertical resolution of the airborne radar observations, and therefore worth demonstrating, but we do not necessarily anticipate retrieving a vertical profile of Nw from EarthCARE, which will have coarser 500m vertical resolution.

Line 1: remove second 'of'

Done.

Page 1, line 18: also A. Behrangi, 2012

Added.

Page 1, line 19: Lebsock et al., 2013 is a better reference than Lebsock et al., 2011

Added.

Page 1, Line 20: Stephens et al. only references intensity. Cite Abel and Boutle, 2012 for the DSD.

Added.

Page 2: line 5. I would mention the GPM DPR before bringing up cloudsat. It has increased sensitivity (12 dbz) vs PR (17 dbz).

This brief timeline of spaceborne cloud and precipitation radars was intended to introduce the capabilities of CloudSat's 94-GHz radar for sensing the vertical profile of light rain, including evaporation and drizzle, in contrast to precipitation radars; for brevity, and because CloudSat followed TRMM historically, we prefer not to introduce GPM here.

Page 2: Lines 14-16. CloudSat actually does not use the SRT (as in the Meneghini 1983 definition) method in its operation products. Instead a look-up-table of normalized surface cross section as a function of wind speed and SST from ECMWF analysis. But Lebsock et al. (2011) do use the SRT for cloud/precipitation water path estimates from CloudSat. The SRT can provide a superior estimate when the length scale of precipitation is short. In the next release of cloudsat precipitation products (release 05) cloudsat will use a hybrid method combining the LUT and SRT techniques each used where appropriate.

Thanks for making this distinction; we have clarified that that the surface cross-section can be estimated both from the SRT and from the surface wind speed and temperature.

The statement now reads:

> The path-integrated attenuation (PIA) can be estimated from the the ocean surface backscatter relative to either nearby clear-sky profiles (Meneghini 1983), or calculated from sea surface wind speed and temperature (Haynes 2009). Estimates of PIA are used in the rain retrieval algorithms of both TRMM (Iguchi 2000, Meneghini 2000) and CloudSat (L'Ecuyer 2002, Haynes 2009, Lebsock 2011) over the ocean...

Page 2, line 30: although these approaches have been challenged in practice due to the spectral dependence of the non-uniform-beam-filling and multiple scattering affecting the two frequencies.

That is interesting; however, notwithstanding these challenges, GPM rain retrievals are intended to use dual-frequency radar to retrieve two parameters of the DSD, and a more detailed discussion here is not required to justify the Doppler approach. With some minor changes, this sentence now reads:

> The recent global precipitation measurement mission (GPM; Hou et al. 2014), with the first dual-frequency radar in space, in intended to exploit differences in non-Rayleigh scattering at 35-GHz and 14-GHz to better constrain the rain DSD over land and ocean (Rose et al. 2006).

Page 3: Lines 27/28: should be Lebsock et al., 2011

Updated.

Equation 1: What is the structure of Jc? What is the structure of B? This is where all the magic happens. Also it's really hard to justify a prior in this retrieval. Why do you feel that you need one? And how do you justify it? The prior variance had better be large. Rodgers was doing sounding where you might actually have a moderately reasonable prior constraint. This approach shouldn't A prior of 0.1 mm/hr is going to make it hard to retrieve 10 mm/hr.

Thank you. We have added more detail and references to describe the terms in Equation 1.

As for a prior R, we do apply it with a large prior variance, so that its influence is small for a well-constrained retrieval. However, as we are demonstrating under-constrained ZPIA and Zv retrievals, the choice of prior does have some influence on the results; this sensitivity to the prior and the double-minimum problem is demonstrated in Section 3.

Changes:

To describe Jc and B in more detail, we now write:

> . . .and B is the error covariance matrix of xa in which the diagonal elements are the error variances of x; and Jc(x) provides the capability to apply flatness and smoothness constraints to reduce the effect of observational noise on the state vector (Twomey 1977). Additionally, profiles of retrieved variables can be represented smoothly as a set of cubic spline basis functions (Hogan 2007, and in Section 2.3.3).

To better explain the use of a prior R, we have added the following:

> For all retrievals a prior R of 0.1 mm/h is used. While a prior R is not strictly necessary, it is applied in combination with a large prior uncertainty such that the retrieved R should be relatively insensitive to the prior unless the retrieval is poorly constrained by observations. We note that this value for the prior variance implies that before the measurements are taken we assume there is a 44

Page 6, Line 28. I think the assumption is a necessary one but I think that the justification has less to do with rain rate and more to do rain type. For broad areas of stratiform precipitation I would suppose the invariance is most appropriate but that for any type of convection (light or heavy rain) I'm not so sure.

This distinction is important, and we had over-stated this assumption here; in practice, R is always represented as the basis functions of a cubic spline to allow for vertical variability.

This statement now reads:

> While in moderate stratiform rain R is often close to invariant with height (e.g. Matrosov 2007), processes such as evaporation in the lower atmosphere, and collision–coalescence in warm clouds, will lead to significant variation with height in many contexts. R is therefore represented as the coefficients of a cubic spline basis function with n elements (Hogan 2007); this has the effect of ensuring the vertical profile of R is smoothly varying and continuous with height, and also reducing the number of terms in the state vector.

Page 7, Line 10: This value of k is not consistent with your retrieved rain rate DSD in that bin though is it? I'm not that concerned about this but if I'm correct you should make a note of it.

Matrosov (2008) assumed a Marshall–Palmer distribution in the rain below the melting layer, so there is indeed a mismatch in the DSD assumptions in the rain and in the melting layer,

This is now explicit in the text:

> The estimated attenuation through the melting layer is based on a Marshall–Palmer DSD for the rain below the melting layer (Matrosov 2008), and is not modified to match the retrieved DSD in the profile.

Page 8, Line 5: add citation for the models that use for attenuation. There are many.

Citation to Liebe (1985) added.

Page 8, Line 15: I'm really skeptical of this Matrosov approach. It really depends strongly on steady state rainfall. How often does this happen? In practice in CloudSat data I see that the stuff that really fully attenuates the radar is the convection, where I just wouldn't trust this assumption.

In response to comments from reviewer 1 we have clarified that the necessary assumption for this approach is not that the rain rate is constant, but only that attenuation dominates any observed gradient in apparent radar reflectivity. Subsequently the estimated R from this method is related to the average over the gates in question.

Table 2: a little discussion about where these numbers come from is required. 0.3 dB would be a very good estimate of PIA. From the SRT method the instrument noise alone is probably close to this value. Is the 3 dBZ including the uncertainty in your DSD– Z relationship? Another thing to consider is whether this 3 dBZ uncertainty should be constant with height. In reality uncertainty should grow with depth into the column (e.g. Lebsock and L'Ecuyer, 2011) because any errors you make in your forward modeled attenuation in the range volumes up high is compounded as you descend into the rain column. This becomes an issue when the PIA is order 20 dB like the cases you explore later in the paper.

In practice the results of the ZvPIA retrieval are fairly insensitive to the uncertainties, with the exception of the under-constrained Zv and ZPIA retrievals. The uncertainty in these variables should include both measurement and forward-model error, so in response to several reviewer comments we now use more physically reasonable values: 3 dB for radar reflectivity,

1.0 m/s for mean Doppler velocity,

0.5 dB for PIA

Changes:

All figures have been re-run with the updated uncertainties. The changes are small, especially for the ZvPIA retrievals that are well-constrained by observations. Table 2 is updated, and the values of the uncertainties updated in the text.

The following discussion has been added:

> We have found that the weighting of errors between radar reflectivity and PIA is quite important for the retrieved rain rate, and that if only instrument errors are included the retrieval is not sufficiently constrained by PIA. This is believed to be because attenuation affects all forward-modelled radar

reflectivity measurements in the same way, leading to them having strong error correlations. Error correlations are not accounted for in the R matrix, since they are profile-dependent and difficult to estimate, which can lead to the radar reflectivity measurements being over-weighted in the retrieval. To overcome this, we take the common approach (e.g. Weston et al. 2014) of inflating the reflectivity errors (and in our case somewhat reducing the errors in PIA) to better balance the information coming from the reflectivity profile and from PIA.

Fig 5a and elsewhere: I can't understand why the Zv retrieval is not matching the radar reflectivity. Doesn't Zv mean that both radar reflectivity and mean Doppler are used to constrain the solution. It looks like only Doppler is used in these plots.

The Zv retrieval does make use of both radar reflectivity and mean Doppler velocity, but is under-constrained, and therefore prone to bimodal errors as illustrated in Section 3.

In this case the Zv retrieval starts from the prior R of 0.1 mm/h, and stays in a low-R state. While D0 is constrained by the Doppler, without PIA R is under-estimated, and therefore—without including attenuation in the forward-model—the retrieval has difficulty resolving the gradient of Z. Conversely, starting from a higher prior R improves the performance of the Zv retrieval in this case, but would lead to high-R retrievals in the light rain profiles.

This sensitivity to the prior is not evident for the ZvPIA retrievals, which are well constrained.

onclusions: The idea that mean Doppler will help with light rainfall retrievals over land is good but I worry that you often won't know whether you are looking at light rainfall or heavier rainfall that appears light because it is attenuated. This process will need to be automated in a retrieval algorithm and it doesn't seem straightforward. Also, the signal in the Doppler is not all that large relative to the uncertainties that are expected.

It's true that this will be a challenge, but we think the results shown here are promising. The synthetic profile in Section 3, and the moderate rain profiles with PIA 20 dB in Case 1 showed that the Zv retrieval can sometimes be used to distinguish weakly and strongly attenuated profiles based on the profiles of Z and v; however, it's true that this will not always be sufficient in practice.

It may be necessary to estimate PIA over land (even with large measurement error) to help identify strong attenuation, or to assume Nw in the retrieval, so that t. A simple test for weakly attenuated profiles might be to identify profiles in which the maximum reflectivity is less than some threshold.

Changes:

A "further work" statement is added in the third-to-last paragraph on the contribution of Doppler to the retrieval, while the more optimistic statement about retrievals over land in the final paragraph has been removed.

Conclusions: Won't Doppler be affected by Multiple scattering for EarthCARE? I haven't done any calculations of this but I wonder how this might complicate things.

Multiple scattering is indeed expected to affect the Doppler for EarthCARE (Battaglia and Tanelli, 2011). We have added the following:

Changes:

The brief mention of multiple scattering in Section 2.4 now reads:

> Multiple scattering effects on radar and lidar backscatter can be estimated within CAPTIVATE using Hogan (2008). Radar reflectivity enhancement due to multiple scattering is especially relevant to spaceborne radar measurements at millimeter wavelengths (Battaglia 2005), and the effects on Doppler radar measurements are expected to include both enhanced spectral broadening and modified mean Doppler velocity (Battaglia 2011); however, with the narrower beam of the airborne radar used in this study we can assume multiple scattering effects are negligible (Battaglia 2007).

In the conclusion we now reiterate the challenges of applying these methods to EarthCARE, including multiple scattering and measurement error.

Interactive comment on Atmos. Chem. Phys. Discuss., https://doi.org/10.5194/acp-2017-280, 2017.

Atmos. Chem. Phys. Discuss.,
https://doi.org/10.5194/acp-2017-280-AC3, 2017

Atmospheric Chemistry and Physics
Discussions

Interactive comment on "Improved rain-rate and drop-size retrievals from airborne and spaceborne Doppler radar" *by* Shannon L. Mason et al.

Shannon L. Mason et al.

s.l.mason@reading.ac.uk

Received and published: 6 July 2017

We thank the reviewers for their constructive comments, and hope that our responses have helped to improve the paper.

A common thread across the reviews was a request for more justification of the retrieval of a height-invariant Nw, and for evaluation of the retrievals through the vertical profile. In response we have added Figs. 5, 9 & 12 evaluating the averaged vertical profile of retrieved and forward-modelled variables in key precipitation regimes: moderate stratiform rain (case 1), light stratiform rain with strong evaporation (case 2), and moderate warm rain (case 3).

In evaluating the instances where the constant-Nw representation was not able to re-

produce the profile of 9.6 GHz radar observations, we thought it worthwhile to add a demonstration of the retrieval in which Nw is represented as a linear gradient (Section 6). We show that introducing another degree of freedom allows us to resolve some of the variations in the DSD through the profile as expected for collision-coalescence, and that these changes lead to an improved ability to forward-model the independent 9.6 GHz radar measurements. This is possible with the high vertical resolution of the airborne radar observations, and therefore worth demonstrating, but we do not necessarily anticipate retrieving a vertical profile of Nw from EarthCARE, which will have coarser 500m vertical resolution.

General comments:

1. Page 11, line 5: Since you don't have independent measurements to validate your algorithm, you have elected to use Z9.6 and V9.6 as an indirect validation, which is OK but is certainly a limitation in the paper. It would be great to make the most out of it. So I wonder why you have decided not to show the whole vertical distribution (and maybe difference plots). That would characterize the errors in a more exhaustive way. A major improvement to the paper would be to demonstrate that with the limited validation you have, you can show that the vertical distribution is captured.

Our instinct was to limit the propagation of figures by comparing multiple retrievals on a single axes: hence the comparison of ZPIA, Zv and ZvPIA retrievals at a selected level above sea level; however, we agree that this didn't allow for sufficient evaluation of the vertical distribution.

Plots of the full vertical curtain plots for each retrieval (ZPIA, Zv, ZvPIA) tend to look quite similar, while the difference plots highlight errors at the tops and the bottoms of the profile and in both cases, we felt these would significantly increase the number of figures and be relatively difficult to interpret.

We have therefore included averaged vertical profiles of observed and forward-modelled radar measurements and retrieved R, D0 and Nw over selected rain regimes for each case. The new Fig. 5 shows the moderate rain profiles of Case 1, Fig. 9 is for all of Case 2, and Fig. 12 shows the moderate warm rain profiles from Case 3. The new Fig. 5 replaces a previous figure showing a selected vertical profile, but illustrates much the same major points.

As discussed in responses to general comment 2 and specific comment 8, this evaluation in the vertical profile allows for some additional insights into how the DSD is resolved with height, and the limits of the constant-Nw assumption.

2. Discussion on case study 2, Fig. 8: No comment on the vertical distribution of D0 for that difficult case? In evaporation conditions is it realistic to see D0 decreasing at lower altitudes? The fact that Nw is held constant should be an issue here, as one might expect Nw to strongly diminish lower in height, and maybe Do increase due to removal of the smaller drops evaporating? That is one illustration of my general comment 1. You need to show the vertical distribution, not a selected height, because it does not tell the full story.

We now make a more detailed evaluation of the vertical profile for all cases. For Case 2 (Fig. 9) the forward-modelled mean Doppler velocity at both 94-GHz and 9.6-GHz are underestimated, but close to observations throughout the vertical profile, however the 9.6-GHz radar reflectivity is significantly underestimated in the lowest part of the profile, where evaporation is significant. This suggests D0 is well-constrained by the Doppler, and that the assumption of constant-Nw is leading to errors in the forward-modelled 9.6-GHz radar reflectivity.

In response to this and other questions about the assumption of constant-Nw, we have added Section 6, exploring the possibility of retrieving some additional information about the vertical structure: a retrieval of a linear profile of Nw is demonstrated for the warm rain case, in which we would expect collision–coalescence to lead to a decrease in drop number concentration toward the surface, combined with the increase in drop size.

For Case 2, if Nw is free to be represented by any linear profile (attached), we can improve the fit between forward-modelled 9.6-GHz radar reflectivity, with the retrieved Nw decreasing toward the surface and D0 increasing somewhat as the smallest drops evaporate, as you have suggested. This comes at the cost of an overestimate of 9.6-GHz mean Doppler velocity; this may indicate that the assumption of a constant shape factor mu=5 does not hold as the DSD becomes more monodisperse.

3. Page 17, lines 23-24: You say that in this study you have used measurements to investigate the prospects for improved global rain rate retrievals from spaceborne Doppler radar. However in order to study that more completely you could have chosen to simulate from these aircraft observations what EarthCARE would actually measure, and whether you would be able to get similar results between degraded spaceborne measurements and higher-resolution higher-quality airborne measurements. I feel this piece of work is missing to really make that claim. In that respect I would remove mention of "spaceborne" in the title of the paper, not to give the impression that you are actually improving satellite rain rates with this technique, as I don't think you showed that.

This is fair enough; the title has been changed.

Specific comments:

1. Page 1, line 11: separate "between" and "light".

Done

2. Page 3, line 10, "...unattenuated wavelength...". This is incorrect, there is still large attenuation at X-band. This needs to be rephrased and errors associated with potential X-band attenuation assessed.

That's true. Attenuation in the X-band is included in the radar forward-model.

Changes:

The line in question now reads "…at a less attenuated wavelength…", and further details has been added in Section 2.4 to make it clear that both W- and X-band radar attenuation are accounted for in the forward-model.

3. Page 3, line 15, "dual-radar" : do you mean dual-frequency radar?

Yes I did; fixed.

4. Section 2.3.4 title : What about 94 GHz attenuation due to graupel or hail ? Something needs to be said about that in this paper.

We have focused on stratiform precipitation here, where Doppler is expected to be most useful.

We expect that for EarthCARE a pre-check will flag convective precipitation, where

graupel and hail are expected, and in which the radar is quickly attenuated.

Changes:

Title changed to "Stratiform precipitation melting layer"

We note that "Melting of graupel and hail, usually associated with convective precipitation, are not considered in this melting layer model."

5. Page 8, line 5 : "assume multiple scattering effects are negligible...". You should probably explain why you think that is reasonable (very small beamwidth). A comment is also needed to explain that this would need to be done in a spaceborne application.

In response to this and comments from other reviewers, in this section we now describe the assumption of negligible multiple scattering for the airborne data, as well as the expected effects of MS on satellite Doppler radar.

Changes:

This section now reads:

> Multiple scattering effects on radar and lidar backscatter can be estimated within CAPTIVATE using Hogan (2008). Radar reflectivity enhancement due to multiple scattering is especially relevant to spaceborne radar measurements at millimeter wavelengths (Battaglia et al 2005), and the effects on Doppler radar measurements are expected to include both enhanced spectral broadening and modified mean Doppler velocity (Battaglia et al 2011); however, with the narrower beam of the airborne radar used in this study we can assume multiple scattering effects are negligible (Battaglia et al. 2007).

6. Page 8, line 24: "as 3 dBZ, and as 0.5ms−1 for mean Doppler ...". This seems large for reflectivity and too small for Doppler velocity. Vertical air motions can be 1-2 ms-1 in the lower troposphere easily in the clouds you are interested in ... That brings up a question you need to address (sorry...): how sensitive to this value are the results?

The ZvPIA retrievals are relatively insensitive to these uncertainties, however the Zv and ZPIA retrievals, being under-constrained, are significantly more sensitive to the choice of values.

In response to this and other comments we have reproduced the retrievals using more relaxed values that better fit with the expected combined measurement and forward-model errors: 3 dB for Z, 1.0 m/s for mean Doppler velocity, and 0.5 dB for PIA.

The following discussion has been added to this section:

> We have found that the weighting of errors between radar reflectivity and PIA is quite important for the retrieved rain rate, and that if only instrument errors are included the retrieval is not sufficiently constrained by PIA. This is believed to be because attenuation affects all forward-modelled radar reflectivity measurements in the same way, leading to them having strong error correlations. Error correlations are not accounted for in the R matrix, since they are profile-dependent and difficult to estimate, which can lead to the radar reflectivity measurements being over-weighted in the retrieval. To overcome this, we take the common approach (e.g. Weston et al. 2014) of inflating the reflectivity errors (and in our case somewhat reducing the errors in PIA) to better balance the information coming from the reflectivity profile and from PIA.

7. Page 8, line 27, " .. by liquid water...". What about melting ice, graupel, hail ?

This was intended to focus specifically on the interpretation of profiles of apparent radar reflectivity in rain; however, it is true that we had not sufficiently addressed the attenuation due to other hydrometeors, and this is now discussed in more detail in Section 2.3.4 on the melting layer (in response to comment 4).

8. Page 14, line 31-32: What about at lower height? I would expect that if the Nw assumption is not satisfied lower down in the evaporating area, then D0 should have more errors and then Z(9.6 GHz) would be less good. It would actually be more interesting to show the whole vertical distribution instead of extracting one height for all these plots to demonstrate if the Nw assumption does create discrepancies on the vertical distribution of Z9.6. Hence my general comments 1 and 2.

Indeed, the errors in 9.6-GHz reflectivity are largest toward the bottom of the profile where evaporation is most significant. Figures 5, 9 and 12 showing the averaged vertical profile for each case have been added, allowing evaluation of the retrieval against the radar variables at all heights.

In light of this and other questions about the retrieval of constant-Nw, we have added a brief section (Section 6) to the paper, to investigate the retrieval of more a linear gradient of Nw, which improve the fit to 9.6-GHz observations.

9. Section 4.3.1, title: I think you could go to 12:46 for your comparisons? Why did you stop at 12:45 ?

This was a pretty arbitrary division based on cloud-top height; however, we agree 12:46 seems like a more suitable cutoff based on radar reflectivity and PIA. The time periods have been changed in the title and discussion, and the period 12:41–12:46 is the subject of the added Section 6 on the retrieved profile of Nw.

Interactive comment on Atmos. Chem. Phys. Discuss., https://doi.org/10.5194/acp-2017-280, 2017.

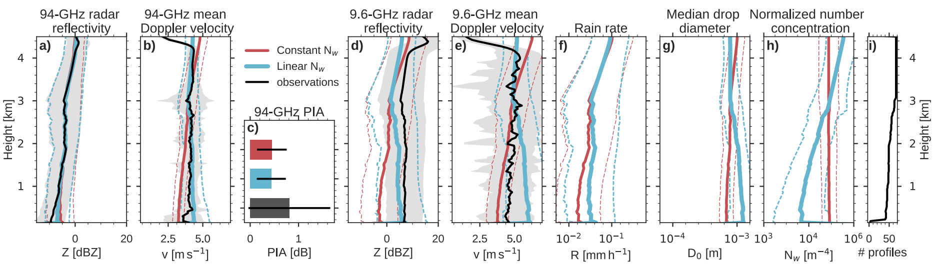

Fig. 1. Comparison of linear-Nw and constant-Nw retrievals over the evaporating cold rain regime (Case 2); a similar figure for Case 3 is now included in Section 6 of the manuscript.

List of changes

Improved rain-rate and drop-size retrievals from airborne ~~and spaceborne~~ Doppler radar

Shannon L. Mason[1,2], J. Christine Chiu[1,2], Robin J. Hogan[1,3], and Lin Tian[4,5]

[1]Department of Meteorology, University of Reading, Reading, UK
[2]National Centre for Earth Observation, University of Reading, Reading, UK
[3]European Centre for Medium-range Weather Forecasts, Reading, UK
[4]NASA Goddard Space Flight Centre, Greenbelt MD, USA
[5]Morgan State University, Baltimore MD, USA

Correspondence to: Shannon Mason (s.l.mason@reading.ac.uk)

Abstract. Satellite radar remote-sensing of rain is important for quantifying ~~of~~ the global hydrological cycle, atmospheric energy budget, and many microphysical cloud and precipitation processes; however, radar estimates of rain rate are sensitive to assumptions about the raindrop size distribution. The upcoming EarthCARE satellite will feature a 94 GHz Doppler radar alongside lidar and radiometer instruments, presenting opportunities for enhanced global retrievals of the rain drop size distribution.

In this paper we demonstrate the capability to retrieve both rain rate and a parameter of the rain drop size distribution from an airborne 94 GHz Doppler radar using CAPTIVATE, the variational retrieval algorithm developed for EarthCARE radar–lidar synergy. For a range of rain regimes observed during the Tropical Composition, Cloud and Climate Coupling ~~(TC4)~~ field campaign in the eastern Pacific in 2007, we explore the contributions of Doppler velocity and path-integrated attenuation (PIA) to the retrievals, and evaluate the retrievals against independent measurements from a second, less attenuated, Doppler radar aboard the same aircraft. Retrieved drop number concentration varied over five orders of magnitude between

light rain from melting ice, and warm rain from liquid clouds. Doppler velocity can be used to estimate rain rate over land, and retrievals of rain rate and drop number concentration are possible in profiles of light rain over land; in moderate warm rain, drop number concentration can be retrieved without Doppler velocity. These results suggest that EarthCARE rain retrievals enhanced by~~facilitated by~~ Doppler radar capability will make substantial improvements to the global understanding of the interaction of clouds and precipitation.

1 Introduction

Satellite remote sensing of rain is important for quantifying the global water and energy cycles. Even light rain and drizzle make significant contributions to global precipitation (Haynes et al., 2009; Berg et al., 2010; Behrangi et al., 2012), while profiling measurements can be used to estimate the vertical transfer of latent heat (Nelson et al., 2016) and microphysical processes (Lebsock et al., 2013; Wood et al., 2009). The intensity and drop size distribution (DSD) of rain are related to persistent errors in weather and climate models, which frequently produce excess drizzle from shallow maritime clouds (Stephens et al., 2010; Abel and Boutle, 2012). Improved instrumentation and retrieval algorithms for the satellite remote sensing of rain are therefore priorities for earth observation and model evaluation.

The first spaceborne cloud and precipitation radars facilitated significant advances in the detection and measurement of rain, especially over the oceans. The 14 GHz precipitation radar aboard the tropical rainfall measurement mission (TRMM; Kummerow et al., 1998) measured moderate and heavy precipitation in the tropics. The more sensitive 94 GHz cloud profiling radar aboard CloudSat (Stephens et al., 2002) is capable of measuring very frequent light rainfall not detected by TRMM, which amounts to 10 % of the total tropical maritime precipitation (Berg et al., 2010). CloudSat measurements of the profile of light rain have shown that around 70 % of marine precipitation falls as drizzle, 50 – 80 % of which evaporates before reaching the surface (Rapp et al., 2013). The high sensitivity of 94 GHz radar allows profiling measurements of light rain and drizzle, at the cost of significant radar attenuation in moderate to heavy rain.

The retrieval of rain rate from a profile of apparent radar reflectivity requires knowledge of the attenuation of the radar beam.~~To reliably estimate rain rates from profiles of radar reflectivity, the attenuation of the radar beam due to liquid hydrometeors must be quantified.~~ The path-integrated attenuation (PIA) can be estimated from the~~ reduction of~~ the ocean surface backscatter relative to nearby clear-sky profiles (Meneghini et al., 1983), or calculated from sea surface wind speed and temperature (Haynes et al., 2009). Estimates of PIA are~~PIA estimated from this surface reference method is~~ used in the rain retrieval algorithms of both TRMM (Iguchi et al., 2000; Meneghini and Liao, 2000) and CloudSat (L'Ecuyer and Stephens, 2002; Haynes et al., 2009; Lebsock and L'Ecuyer, 2011) over the ocean; however, the surface backscatter over the land is much more variable and difficult to characterise. Consequently operational CloudSat data products currently provide only rain detection over land, and not rain rate estimates (e.g. Haynes et al., 2009; Lebsock and L'Ecuyer, 2011). Additional radar measurements that facilitate rain rate estimates over land would offer a significant improvement~~significant improvements~~ over existing satellite capabilities.

Estimates of rain rate from limited radar measurements rely upon assumptions about the rain DSD. While the statistical properties of rain DSDs have been found to be broadly consistent and robust over time, whether measured in situ (Marshall and Palmer, 1948; Tokay and Short, 1996) or estimated by radar remote-sensing (Wilson et al., 1997; Illingworth and Blackman, 2002), the instantaneous microphysical properties of rain are observed to vary over many orders of magnitude (Testud et al., 2001). Assumptions about the drop number concentration in particular have been identified as a major source of uncertainty in TRMM and CloudSat estimates of rain rate (Iguchi et al., 2009; Lebsock and L'Ecuyer, 2011). To improve upon the uncertainties of satellite remote-sensed rain rate, there is a need for additional radar measurements with which to better characterise the rain DSD.

There are two approaches to improving rain retrievals with additional observations from satellite radars, both to assist in estimating rain rate over land, and to better constrain the rain DSD. The recent global precipitation measurement mission (GPM; Hou et al., 2014), with~~uses~~ the first dual-frequency radar in space, aims to exploit differences in non-Rayleigh scattering at 35 GHz and 14 GHz~~,~~ to better constrain the rain DSD over land and ocean (e.g. Rose and Chandrasekar, 2006). Another approach is to use Doppler radar to measure the terminal fallspeed of raindrops, which is related to drop size. The Doppler spectrum has been used in ground-based radar retrievals to resolve vertical air motion (Atlas et al., 1973; Firda et al., 1999; O'Connor et al., 2005), distinguish cloud from precipitation (Frisch et al., 1995; Luke and Kollias, 2013), and to understand warm rain processes (Kollias et al., 2011b, a). Unfortunately in spaceborne radar applications the Doppler spectrum is broadened by the lateral motion of the radar platform with respect to the scattering hydrometeors (Illingworth et al., 2015), which distorts the higher moments of the Doppler spectrum; consequently, only radar reflectivity, PIA, and mean Doppler velocity measurements are useful for spaceborne Doppler radar retrievals.

The EarthCARE satellite will feature a 94 GHz Doppler radar along with lidar and radiometers, for synergistic retrievals of clouds, aerosols and precipitation (Illingworth et al., 2015). In this study we develop a method for making an improved estimate of rain rate by simultaneously retrieving information about the DSD from an airborne 94 GHz Doppler cloud radar. We use a variational retrieval methodology developed for radar–lidar synergy from EarthCARE (Illingworth et al., 2015), and exploit mean Doppler velocity to retrieve the raindrop number concentration. NASA's high-altitude ER-2 aircraft provides an ideal platform for satellite instruments and retrievals; we use ER-2 measurements from the Tropical Composition, Clouds and Climate Coupling field campaign (TC4) off Costa Rica and Panama in 2007 (Toon et al., 2010). A second 9.6 GHz~~10 GHz~~ Doppler radar aboard ER-2 provides independent measurements at a less attenuated~~an unattenuated~~ wavelength, with which to evaluate the retrievals.

The structure of this paper is as follows. We first describe the aircraft measurements, the synergistic classification of hydrometeors, and the retrieval method (Section 2). The ambiguities of retrieving rain rate from attenuated radar profiles are discussed using synthetic measurements (Section 3), before 94 GHz radar retrievals of rain rate and drop number concentration are presented for three case studies, and the retrievals are evaluated against independent radar measurements at an unattenuated wavelength (Section 4). We briefly consider applications of the dual-frequency radar~~-radar~~ retrievals (Section 5), and the retrieval of more complex variations in the DSD through the vertical profile (Section 6), before summarising our key findings with a view to applications to EarthCARE retrievals (Section 7).

2 Data and retrieval methodology

2.1 Measurements used in the retrieval

The observations are from NASA's high altitude ER-2 aircraft during the TC4 experiment conducted over the tropical eastern Pacific in July and August 2007 (Toon et al., 2010). ER-2 flies above the tropopause at an altitude of $20\,\mathrm{km}$ with a cruise speed around $200\,\mathrm{m\,s^{-1}}$. We analyse measurements from straight flight legs over the ocean, and average all measurements over $5\,\mathrm{s}$ intervals, so that each pixel of radar–lidar data has a $1\,\mathrm{km}$ along-track footprint.

The $94\,\mathrm{GHz}$ ($3.2\,\mathrm{mm}$ wavelength) cloud radar system (CRS; Li et al., 2004) and $9.6\,\mathrm{GHz}$ ($3.1\,\mathrm{cm}$ wavelength) ER-2 Doppler radar (EDOP; Heymsfield et al., 1996) measure radar reflectivity factor and mean Doppler velocity with a vertical gate spacing of $37.5\,\mathrm{m}$. The $94\,\mathrm{GHz}$ radar reflectivity factor is calibrated against the $9.6\,\mathrm{GHz}$ radar near cloud-top (McGill, 2004), and the mean Doppler velocity measurements are calibrated using the surface signal (Li et al., 2004). The path-integrated attenuation (PIA) of the $94\,\mathrm{GHz}$ radar is estimated over the ocean using the surface reference technique (L'Ecuyer and Stephens, 2002; Lebsock and L'Ecuyer, 2011). In this study we focus on the retrieval of rain from the $94\,\mathrm{GHz}$ cloud radar, and use the $9.6\,\mathrm{GHz}$ radar for evaluation.

The cloud physics lidar (CPL; McGill et al., 2002) measures attenuated backscatter at $355\,\mathrm{nm}$, $532\,\mathrm{nm}$ and $1064\,\mathrm{nm}$, with linear polarisation ratio measured at the $1064\,\mathrm{nm}$ wavelength. In this study the $532\,\mathrm{nm}$ attenuated backscatter is used in the classification scheme to detect cloud top and to retrieve overlying ice cloud and liquid layers when the lidar signal is not fully attenuated.

The MODIS airborne simulator (MAS; King et al., 1996) and MODIS/ASTER airborne simulator (MASTER; Hook et al., 2001) imaging radiometers measure infrared (IR) and visible channels. Three visible channels are combined to create composite images of the case studies. Due to a failure in the MAS instrument, the MASTER instrument flew aboard ER-2 as a replacement after 29 July 2007 (Toon et al., 2010); the channels used in this study are common to both instruments.

Supplementary environmental data are required to complete the retrieval. Atmospheric temperature, humidity and ozone concentration are used to classify hydrometeor thermodynamic phase and estimate radar and lidar attenuation due to atmospheric gases. These variables are interpolated onto the flight track from the European Centre for Medium-Range Weather Forecasts (ECMWF) Interim Re-Analysis (ERA-Interim; Dee et al., 2011).

2.2 Target classification

Prior to the retrieval the contents of each pixel are classified based on a synthesis of radar and lidar measurements. We exploit the instruments' complementary sensitivities to different classes of hydrometeors to infer the presence of liquid cloud, rain and drizzle, and ice. This approach to radar–lidar target classification is similar to that described for CloudSat–CALIPSO in Ceccaldi et al. (2013), however the categories are simplified in this analysis.

A trade-off in radar and lidar remote sensing is that the hydrometeors with the strongest backscatter also strongly attenuate the beam, weakening its penetration. The sensitivity of lidar to small ice crystals and cloud droplets makes it suited to detecting optically thin ice and liquid cloud, but lidar is therefore quickly attenuated in all but the optically thinnest clouds. In contrast, cloud radar is most sensitive to large hydrometeors such as ice aggregates and raindrops, and becomes fully attenuated in heavy rain. With the synergy of the two instruments we can use radar to detect optically thick clouds and light to moderate rain, while lidar detects optically thin ice and liquid cloud-tops missed by the radar.

The thermodynamic phase of targets is primarily determined by the atmospheric temperature from reanalysis, with further distinctions made using thresholds of radar and lidar measurements. At temperatures colder than $-40\,°\mathrm{C}$ all targets are classified as ice, and at all temperatures warmer than $0\,°\mathrm{C}$ as "warm" liquid cloud or precipitation. Rain and drizzle is inferred at temperatures greater than $0\,°\mathrm{C}$ from radar reflectivities greater than $-15\,\mathrm{dBZ}$ (as in Haynes et al., 2011, and others), and may be colocated with warm liquid clouds detected by lidar. In stratiform precipitation we assume that the transition from ice to liquid precipitation occurs in a shallow melting layer (see Section 2.3.4); however, in convective precipitation strong attenuation due to melting hail and tends to extinguish the 94 GHz radar. Between $-40\,°\mathrm{C}$ and $0\,°\mathrm{C}$ the thermodynamic phase of cloud water can be ice, supercooled liquid or, where the two coexist, mixed-phase. First all targets detected by radar are classified as containing ice, due to the sensitivity of that instrument to the largest particles. Then liquid and ice as detected by lidar are distinguished based on the vertical gradient of lidar backscatter, which is higher in liquid cloud (Ceccaldi et al., 2013); this method of distinguishing liquid cloud is consistent with the method of Yoshida et al. (2010) using the lidar depolarization ratio. Where radar detects ice and lidar detects liquid, mixed-phase cloud is diagnosed.

The vertical structure and thermodynamic phase of clouds provide constraints on the retrieval of cloud and precipitation properties, but the entire profile is frequently not detectable by both instruments. Therefore the lidar is used to retrieve liquid clouds, but the presence of liquid cloud droplets is an uncertainty in the classification scheme where only radar measurements are available. The lidar is included in the present work for its contribution to the classification of cloud through the vertical profile, and for measuring the water content at cloud-top; however, the radar is the dominant instrument for the retrieval of rain. As a result of the uncertain presence of liquid clouds within rainy profiles, the path-integrated attenuation of the radar that is attributed to rain may be partially due to undiagnosed liquid cloud. Finally, in profiles where the radar is fully attenuated by heavy rain, we assume that rain is continuous to the surface.

2.3 Retrieval methodology

Radar–lidar retrievals of profiles of rain and ice cloud are made using the Clouds Aerosols and Precipitation from mulTiple Instruments using a VAriational TEchnique (CAPTIVATE) algorithm, an earlier version of which was outlined in Illingworth et al. (2015). In this section we first describe the CAPTIVATE framework, then the main components pertinent to this study: the cost function, the state vector for rain, and the radar forward model. The retrieval is made by iteratively minimizing the cost function to find the state vector that corresponds to the smallest difference between observed and forward-modelled measurements. The state vector consists of the quantities or parameters of the rain DSD selected as retrieved variables. The forward models are used to estimate the measured variables given the state; the relevant measurements are radar reflectivity factor, PIA, and mean Doppler velocity. In this study we focus on the rain retrieval; details for other hydrometeors will be provided in subsequent papers.

2.3.1 Retrieval framework

The CAPTIVATE algorithm provides a framework for a variational, or optimal estimation, approach (Rodgers, 2000) to the inverse retrieval of the profiles of rain, ice and snow, liquid cloud and aerosols from one or more vertically-pointing active and passive instruments. CAPTIVATE is novel in that the measurements used and state variables retrieved are easily configurable, so that the same retrieval algorithm can be applied to spaceborne, airborne and ground-based measurements~~applications~~. The treatment of retrieved state variables and the vertical representation of each class of hydrometeor can also be modified as appropriate. The variational approach allows for a robust treatment of uncertainties in the retrieval, subject to the appropriate selection of observational uncertainties, forward-model errors and physical constraints.

2.3.2 Cost function and minimization

Here we present a general description of the CAPTIVATE retrieval; justifications for the settings used in study are made in later subsections. The retrieval is made for each profile by iterating to find a state vector that minimizes a cost function, given by

$$J = \frac{1}{2}\delta\mathbf{y}^{\mathrm{T}}\mathbf{R}^{-1}\delta\mathbf{y} + \frac{1}{2}\delta\mathbf{x}^{\mathrm{T}}\mathbf{B}^{-1}\delta\mathbf{x} + J_c(\mathbf{x}) \tag{1}$$

where $\delta\mathbf{y} = \mathbf{y} - \mathbf{y}^f$ is the difference between the observed ($\mathbf{y}$) and forward-modelled ($\mathbf{y}^{\mathbf{f}}$) measurements; $\mathbf{R}$ is the error covariance matrix of $\delta\mathbf{y}$, the sum of the error covariance matrices of the observations and the forward model; $\delta\mathbf{x} = \mathbf{x} - \mathbf{x}^a$ is the difference between the state ($\mathbf{x}$) and its a priori estimate ($\mathbf{x}^a$), and $\mathbf{B}$ is the error covariance matrix of $\mathbf{x}^a$~~the a priori~~ in which the diagonal elements are the error variances of $\mathbf{x}$; and $J_c(\mathbf{x})$ provides the capability to apply~~represents the~~ flatness~~physical~~ and smoothness~~ing~~ constraints to reduce the effect of observational noise on the state vector (Twomey, 1977).~~on the state vector.~~ Additionally, profiles of retrieved variables can be represented smoothly as a set of cubic spline basis functions (Hogan, 2007, and in Section 2.3.3). The minimization of the cost function is carried out by iterating on the state vector beginning from the priors, in the direction of the first and second derivatives of the cost function (the Levenberg-Marquadt method; Rodgers, 2000).

2.3.3 Rain state variables

The rain DSD is given by a normalized Gamma function, of the form

$$N(D) = N_w \frac{\Gamma(4)}{3.67^4} \frac{(3.67+\mu)^{4+\mu}}{\Gamma(4+\mu)} \left(\frac{D}{D_0}\right)^{\mu} \exp\left(\frac{-(3.67+\mu)D}{D_0}\right). \tag{2}$$

This formulation is a function of three independent, physically meaningful parameters for the shape μ, median drop size D_0, and drop number concentration N_w of the DSD (Testud et al., 2001; Illingworth and Blackman, 2002). The shape factor μ is of secondary importance to D_0 and N_w in terms of the radar reflectivity (Testud et al., 2001), and is poorly constrained by observations (e.g. Moisseev and Chandrasekar, 2007). In this retrieval we use $\mu = 5$, a value derived from both radar and distrometer studies (Wilson et al., 1997; Illingworth and Blackman, 2002). This simplifies the DSD to a 2-parameter function of D_0 and N_w. The uncertainty due to the assumption of fixed-μ DSD is estimated to be $\pm 15\,\%$ of the rain rate (Wilson et al., 1997), and is included in the uncertainty estimates of the retrieved quantities.

Our primary state variable is the rain rate,

$$R = \frac{\rho_w \pi}{6} \int_0^\infty N(D) D^3 v(D)\, dD \quad [\mathrm{kg\,m^{-2}\,s^{-1}}], \tag{3}$$

from the third moment of the DSD where ρ_w is the density of liquid water, $v(D)$ is the raindrop terminal velocity as a function of drop size from Beard (1976) corrected for air density through the vertical profile. Hereafter we scale R by a factor of 3600 to express rain rate in units of $\mathrm{mm\,h^{-1}}$. For all retrievals a prior R of $0.1\,\mathrm{mm\,h^{-1}}$ is used. While a prior R is not strictly necessary, it is applied in combination with a large prior variance ($\sigma(\ln R) = 4.0$), such that the retrieved R is relatively insensitive to the prior unless the retrieval is poorly constrained by observations. We note that this value for the prior variance implies that before the measurements are taken we assume there is a $44\,\%$ chance of R lying between 0.01 and $1.0\,\mathrm{mm\,h^{-1}}$, and a $56\,\%$ chance R is outside these limits.

The second state variable is N_w, so that one state variable is an integral over the DSD and the second is a parameter of the DSD. Additional state variables increase the degrees of freedom of the retrieval, and require more information from observational variables to constrain the retrieval. Therefore we retrieve a single value of N_w for each profile, with the physical interpretation of representing N_w as constant with height, or as the vertically-averaged value. The representation of N_w as constant with height is not expected to be borne out in cases where evaporation or collision-coalescence processes modify the drop number concentration through the vertical profile. We take as the prior N_w the number concentration intercept of the Marshall and Palmer (1948) DSD, $8 \times 10^6\,\mathrm{m^{-4}}$.~~and assume N_w is constant with height in each profile.~~

When few observational variables are available, a single-parameter retrieval of R can be made by assuming that N_w is constant and equal to its prior~~holding N_w constant~~, reducing the degrees of freedom so that R is a function of D_0 alone. This is called the "R-only" retrieval, and is similar to CloudSat rain rate retrievals in which N_w is assumed constant everywhere. When additional observational variables are available, such as the mean Doppler velocity, there may be sufficient information to also retrieve N_w; this is called the R-N_w retrieval.

We use the natural logarithms of R and N_w as the state variables, with the effect~~to ensure~~ that the values remain positive everywhere and that the algorithm converges in fewer iterations~~faster~~. While in moderate stratiform rain R is often close to invariant with height (e.g. Matrosov, 2007), processes such as evaporation in the lower atmosphere and collision–coalescence in warm clouds will lead to significant variation with height in many contexts. R is therefore represented as the coefficients of a cubic spline basis function with n elements (Hogan, 2007); this has the effect of ensuring the vertical profile of R is smoothly varying and continuous with height, and also reducing the number of terms in the state vector. Table 1 summarises the rain state variables, their prior values and uncertainties, and physical representation~~constraints applied to their representation~~ in each vertical profile. For R-only retrievals the state vector $\mathbf{x}$ for a vertical profile ~~with n elements, or pixels,~~ is given by

$$\mathbf{x} = \ln\left[R_1 \cdots R_n\right]^{\mathrm{T}} \tag{4}$$

while for the R-N_w retrieval the full state vector is

$$\mathbf{x} = \ln \begin{bmatrix} R_1 \cdots R_n & N_w \end{bmatrix}^{\mathrm{T}} \tag{5}$$

where N_w is assumed constant with height in each profile.a single N_w is retrieved per profile. At moderate rain rates, we expect R to be close to invariant with height due to high fallspeeds and negligible evaporation (e.g. Matrosov et al. 2007; however, at low rain rates R may vary vertically, either due to evaporation in the lower atmosphere, or collision–coalescence processes in warm rain (Lebsock 2011). Therefore to reduce noise and ensure smoothly varying rain rate with height, we retrieve each profile of R as the coefficients of cubic spline basis functions.

Table 1. Rain state variables $\mathbf{x_i}$, their prior values $\mathbf{x}_i^a$ and uncertainties $\sigma\left(\mathbf{x}_i^a\right)$. The profile of rain rate R is always retrieved in each profile, while the drop number concentration parameter N_w may be either retrieved or assumed equal to the prior; the melting layer thickness scaling X_m is not retrieved in this study.

$\mathbf{x}_i$	$\mathbf{x}_i^a$	$\sigma\left(\mathbf{x}_i^a\right)$	Vertical representation
$\ln R$	$\ln\left(0.1\,\mathrm{mm\,h^{-1}}\right)$	4.0	Retrieved as the coefficients of a cubic spline basis function, with a spacing of 300 m.
$\ln N_w$	$\ln\left(8\times10^{6}\,\mathrm{m^{-4}}\right)$	3.0	Retrieved as constant with height (R-N_w retrievals), or not retrieved (R-only).
X_m	1.0 km	0.0	Not retrieved in this study.

2.3.4 Stratiform precipitation melting layer

We employ a simplified representation ofrepresent the melting layer in stratiform precipitation by applying radar attenuation between the lowest pixel in each profile classified as ice, and the highest pixel classified as rain, provided the two pixels are contiguous. Melting of graupel and hail, usually associated with convective precipitation, are not considered in this melting layer model. Following Matrosov (2008)Matrosov (2008), it is assumed that the two-way attenuation of the melting layer A is proportional to the rain rate R at the first pixel just below the melting layer, and the two-way path length X_m through the melting layer, such that

$$A = k_m X_m R \quad [\mathrm{dB}] \tag{6}$$

where the melting layer extinction coefficient k_m is $2.2\,\mathrm{dB\,km^{-1}}\left(\mathrm{mm\,h^{-1}}\right)^{-1}$ at 94 GHz and $0.04\,\mathrm{dB\,km^{-1}}\left(\mathrm{mm\,h^{-1}}\right)^{-1}$ at 9.6 GHz. The estimated attenuation through the melting layer is based on a Marshall–Palmer DSD for the rain below the melting layer (Matrosov, 2008), and is not modified to match the retrieved DSD in the profile(Matrosov 2008). The thickness of the melting layer, and therefore the total attenuation, may also depend on the local temperature profile: as sufficient information to retrieve the total melting-layer attenuation may be available from the PIA and the attenuation inferred from the radar reflectivity gradient, we include the variable X_m in the retrieval to represent the effect of melting layer thickness on radar attenuation;

however, in this study ~~the~~ X_m is held constant with a value of $1.0\,\mathrm{km}$~~1~~, allowing us to capture the effect of this uncertainty on the retrieved variables and their errors, without retrieving X_m.

2.3.5 Radar forward model

For a given state vector we estimate the corresponding measurements made by each instrument by forward modelling the scattering behaviour between the sensor and each gate for $94\,\mathrm{GHz}$ and $9.6\,\mathrm{GHz}$ radars, accounting for the effects of atmospheric gases, aerosols and hydrometeors.

The radar reflectivity factor of rain is a function of the sixth moment of the DSD,

$$Z = \int_0^\infty N(D) D^6 \gamma_f(D)\, dD \quad [\mathrm{dBZ}], \tag{7}$$

where γ_f is the Mie–Rayleigh backscatter ratio at the radar frequency f, and is required for both $94\,\mathrm{GHz}$ and $9.6\,\mathrm{GHz}$ radars to account for non-Rayleigh scattering~~ as drop sizes approach the radar wavelength~~. At $94\,\mathrm{GHz}$ the uncertainty of assuming raindrops are spherical Mie scatters is approximately $5\,\%$ in integrated backscatter for a gamma DSD with median drop size $D_0 = 1.5\,\mathrm{mm}$, when compared against estimates for oblate spheroids (e.g. Thurai et al., 2007; Zhang et al., 2001) using the T-matrix method (Mishchenko et al., 1996).

Scattering and attenuation effects are included in the radar forward-model~~All major scattering effects are modelled~~, so that the forward-modelled estimate of the apparent radar reflectivity (Z_a) is directly comparable to observations. Attenuation due to atmospheric gases and the dielectric factor of water are calculated from atmospheric temperature and humidity profiles (Liebe, 1985). Multiple scattering effects on radar and lidar backscatter can be estimated within CAPTIVATE~~for radar and lidar instruments can be estimated~~ using Hogan (2008). Radar reflectivity enhancement due to multiple scattering is especially relevant to spaceborne radar measurements at millimeter wavelengths (Battaglia et al., 2005), and the effects on Doppler radar measurements are expected to include both enhanced spectral broadening and modified mean Doppler velocity (Battaglia and Tanelli, 2011); however, with the narrower beam of the airborne radar used in this study we can assume multiple scattering effects are negligible (Battaglia et al., 2007).~~however for the aircraft measurements used in this study we assume multiple scattering effects are negligible.~~

Radar attenuation due to hydrometeors is quantified at each gate by the extinction coefficient

$$k = \frac{\pi}{4} \int_0^\infty Q(D) N(D) D^2\, dD \quad [\mathrm{m}^{-1}] \tag{8}$$

where $Q(D)$ is the extinction efficiency calculated from Mie theory (Mie, 1908). As for radar reflectivity, the uncertainty in extinction due to assuming spherical drops is less than $2\,\%$ for DSD with D_0 of $1.5\,\mathrm{mm}$. The gradient of extinction can be related to the gradient of apparent radar reflectivity and used to estimate the rain rate as suggested by Matrosov (2007). A second approach to quantifying attenuation due to hydrometeors is to measure the two-way path-integrated attenuation

$$\mathrm{PIA} = 2\frac{10}{\ln 10} \int_0^\infty k\, dz \quad [\mathrm{dB}] \tag{9}$$

for each profile. PIA is estimated from the radar reflectivity at the ocean surface, and used as an observational measurement. Both approaches are implemented simultaneously, so that ~~;~~ whereas the gradient method of Matrosov (2007) is applied only at moderate to heavy rain rates, where it can be assumed that the gradient of apparent radar reflectivity is dominated by attenuation~~required an assumption of constant rain rate with height~~, within the CAPTIVATE variational scheme the gradient of R and k can be estimated simultaneously from the profile of radar reflectivity and the PIA.

Finally the mean Doppler velocity is the reflectivity-weighted mean drop fallspeed,

$$\overline{v}_D = \frac{-\int_0^\infty N(D) D^6 v(D) \gamma_f(D)\, dD}{\int_0^\infty N(D) D^6 \gamma_f(D)\, dD} \quad [\mathrm{m\,s^{-1}}] \tag{10}$$

where the terminal fallspeed of drops $v(D)$ is from the empirical formulation of Beard (1976) scaled to account for air density changes with altitude~~corrected for air density~~, and where positive velocities are toward the ground. The forward-modelled mean Doppler velocity is calculated assuming zero vertical air motion; therefore the difference between the forward-modelled and observed mean Doppler velocities will include a contribution from the vertical air motion, which is treated as an observational uncertainty.

The observed variables, their observational uncertainties and their vertical representation are summarized in Table 2. The uncertainties in the observational variables include both~~estimated uncertainties in the measurements are relaxed somewhat from~~ the specified measurement errors~~uncertainties~~ for the CRS instrument (Li et al., 2004) and the estimated uncertainties in the radar forward model.~~, so that the uncertainty in radar reflectivity is taken as 3 dB, and as $1.0\,\mathrm{m\,s^{-1}}$ $0.5\,\mathrm{m\,s^{-1}}$ for mean Doppler velocity.~~ We have found that the weighting of errors between radar reflectivity and PIA is quite important for the retrieved rain rate, and that if only instrument errors are included the retrieval is not sufficiently constrained by PIA. This is believed to be because attenuation affects all forward-modelled radar reflectivity measurements in the same way, leading to them having strong error correlations. Error correlations are not accounted for in the $\mathbf{R}$ matrix, since they are profile-dependent and difficult to estimate, which can lead to the radar reflectivity measurements being over-weighted in the retrieval. To overcome this, we take the common approach (e.g. Weston et al., 2014) of inflating the reflectivity errors (and in our case somewhat reducing the errors in PIA) to better balance the information coming from the reflectivity profile and from PIA.

Table 2. Observational variables $\mathbf{y_i}$ for Doppler radar, and their estimated uncertainties $\sigma(\mathbf{y_i})$ as used in the retrieval. Apparent radar reflectivity Z_a and mean Doppler velocity $\overline{v}_D$ are measured at each gate, while PIA is estimated from the radar reflectivity over the ocean surface.

$\mathbf{y_i}$	$\sigma(\mathbf{y_i})$	Vertical representation
Z_a	3.0 dB	At each radar gate
$\overline{v}_D$	$1.0\,\mathrm{m\,s^{-1}}$	At each radar gate
PIA	0.5 dB	Integrated for each profile

3 Retrievals of rain rate with attenuated radar

The strong attenuation of 94 GHz radar by ~~liquid water, and especially by~~ rain~~,~~ presents a challenge for retrievals of rain rate from profiles of apparent radar reflectivity (Hitschfeld and Bordan, 1954). For nadir-pointing radars the following ambiguity arises: when the profile of apparent radar reflectivity decreases with range (toward the ground), the decrease could be due to either the attenuation of the radar beam, or to a physical change in the rain DSD (e.g., due to evaporation). These two possibilities each constitute a local minimum in the cost function, so that a profile of evaporating light rain with negligible attenuation may be wrongly identified as a profile of moderate rain with significant attenuation, and visa versa.

To illustrate the double-minimum problem, and to visualise how PIA and Doppler velocity may help resolve this retrieval ambiguity, we use the radar forward model to generate synthetic radar measurements assuming zero observational noise. In practice, measurement error and more complex profiles will introduce further uncertainties in the retrieval than in this synthetic case. Two synthetic profiles of rain are simulated, with constant rain rates of $0.05\,\mathrm{mm\,h^{-1}}$ and $5.0\,\mathrm{mm\,h^{-1}}$ below a level of $5\,\mathrm{km}$, and drop number concentration $N_w = 8\times10^6\,\mathrm{m^{-4}}$, representing a profile of light rain with negligible attenuation, and of moderate rain with strong attenuation, respectively. In making the inverse retrieval of the profile of rain rate corresponding to a given profile of 94 GHz radar reflectivity, multiple solutions may be found depending on the prior rain rate: the low-R and high-R profile of R (Fig. 1a) represent the two minima of the cost function for the retrieval from the radar reflectivity profile (Figs. 1b) corresponding to the $5.0\,\mathrm{mm\,h^{-1}}$ profile of rain (the "truth"). The radar reflectivity alone does not provide sufficient information to differentiate between the two solutions; however, the forward-modelled mean Doppler velocity profile (Fig. 1c) and PIA (Fig. 1d) for the two solutions illustrate how additional observational variables may provide further information with which to resolve the ambiguity. The PIA differs by more than $30\,\mathrm{dB}$ between the two solutions, and is used effectively to differentiate light and moderate rain in CloudSat rain retrievals. The mean Doppler velocity profiles also differ significantly, with the "true" high-R profile varying only slightly with altitude, while the gradient of mean Doppler velocity indicates a reduction of D_0 toward the surface in the low-R profile. An additional advantage of the mean Doppler velocity is that it is not affected by the partial attenuation of the radar.

We can quantify the contribution of the observational variables to resolving ambiguous retrievals using the cost function that is minimized within the variational retrieval scheme. A range of prior rain rates are taken as candidates for the starting-point of the retrieval, and for each prior R the contribution of the observations to the cost function is calculated by

$$J_{\mathrm{obs}} = \frac{1}{2}\sum\frac{\left(\mathbf{y}^f - \mathbf{y}\right)^2}{\sigma_{\mathbf{y}}^2}. \tag{11}$$

which is equivalent to the first term of the cost function in equation (1). We can interpret the curve of J_{obs} (Fig. 1e) as showing the tendency of the retrieval algorithm to converge from any prior R toward a local minimum in the cost function, wherein a steeper curve indicates stronger convergence toward a more robust retrieval. To explore the contributions of the observational measurements, we run the retrievals for the two synthetic profiles with only radar reflectivity observations ("Z-only"), with one additional observational variable ("ZPIA", "Zv"), and with all available observations ("ZvPIA").

For the light rain profile, the cost function for the Z-only retrieval has a secondary minimum at $3.0-4.0\,\mathrm{mm\,h^{-1}}$. The bimodal shape of J shows that the retrieval is sensitive to the choice of prior: if R is less than $1.0\,\mathrm{mm\,h^{-1}}$, the retrieval will converge to the "true" R profile, but if the prior R is greater than $1.0\,\mathrm{mm\,h^{-1}}$ the retrieval will converge on the high-R solution. Conversely, for the moderate rain profile, the Z-only retrieval will converge on a low-R solution if the prior is less than around $0.5\,\mathrm{mm\,h^{-1}}$. These two solutions are compared in Figs. 1a–1d.

The effect of including PIA (dashed lines in Fig. 1e) is strongest for $R > 1.0\,\mathrm{mm\,h^{-1}}$, and this removes any sensitivity to the prior R, while the effect of including Doppler velocity (darker lines in Fig. 1e) is smoother across the full range of R than that of PIA, and dominates at low R where radar attenuation is negligible. When both PIA and Doppler measurements are used the effects are cumulative, and the gradient of J shows even stronger convergence toward the unique solution.

This example provides a simple illustration of the bimodal cost function of an R-only rain retrieval with a strongly attenuating $94\,\mathrm{GHz}$ radar. Without additional observational measurements, a given profile of radar reflectivity may equally be explained by a strongly attenuating profile with constant R, or by a weakly attenuating profile in which R decreases toward the surface. Either PIA or mean Doppler velocity are sufficient to resolve this ambiguity: PIA as a constraint on the total attenuation, and mean Doppler velocity on the profile of D_0. As PIA is typically estimated from the ocean surface backscatter, the availability of mean Doppler velocity to resolve these ambiguities presents an opportunity for Doppler radar estimates of rain rate over land.

4 Retrievals of rain rate and drop number concentration

We now combine~~put to use observations of both~~ PIA and mean Doppler velocity, in addition to radar reflectivity, to make R-N_w rain retrievals from $94\,\mathrm{GHz}$ Doppler radar measurements. Three cases of stratiform rain are selected from two ER-2 flights during TC4 (Fig. 2): two flight legs on 22 July 2007 include rain falling from melting ice, ranging in intensity from virga to heavy showers, and a case of light to moderate warm rain from liquid clouds is observed on 29 July 2007.

For each case the R-N_w retrieval is performed using all available measurements from the $94\,\mathrm{GHz}$ radar: radar reflectivity, mean Doppler velocity and PIA. This "ZvPIA" retrieval is of primary interest for evaluating the full capabilities of the CAPTIVATE retrieval for a Doppler cloud radar; however, we are also interested in the capabilities of a retrieval when one of the observational measurements is not available, or has high observational uncertainty. When mean Doppler velocity measurements are not used (ZPIA), the observational variables are analogous to those available to CloudSat over ocean; however, unlike CloudSat rain retrievals, here we retrieve N_w as well as R. Conversely, when PIA is not used (Zv) the observational variables are similar to those available to a Doppler radar over land, where the land surface cannot be sufficiently characterised to estimate PIA. The ZPIA and Zv retrievals of R-N_w are less constrained by observations than the ZvPIA retrieval, and will therefore demonstrate some bimodal or poorly constrained retrievals similar to those demonstrated for R-only retrievals in Section 3; nevertheless, we include ZPIA and Zv retrievals in order to demonstrate the information provided by the PIA and mean Doppler velocity separately, and to identify situations in which a satisfactory R-N_w retrieval may be made with limited observational variables.

In each case the retrieval is evaluated by forward-modelling all 94 GHz and 9.6 GHz radar variables, whether or not they were assimilated in the retrieval, and comparing against the observations.~~In each case the retrievals are evaluated by forward-modelling independent radar measurements at the unattenuated frequency, and comparing the retrievals at a selected height above sea level.~~

4.1 Case 1: moderate rain from melting ice, 22 July 2007

Stratiform rain from melting ice provides a test of many of the simplifying assumptions made in rain retrievals. At moderate and heavy rain rates we expect R to be close to constant with height, unless significant evaporation is evident (Haynes et al., 2009). N_w may be expected to be close to values deemed typical by Marshall and Palmer (1948) or Testud et al. (2001), i.e. between $2.0 \times 10^6 - 8.0 \times 10^6\,\mathrm{m}^{-4}$, and constant with height (Tokay and Short, 1996). From in situ measurements of stratiform rain we expect median drop sizes ~~in this case~~ to be in the range $1.0 - 1.5\,\mathrm{mm}$ (Tokay and Short, 1996).

Between 15:54 and 16:03 UTC on 22 July 2007 ER-2 overflew approximately $110\,\mathrm{km}$ of precipitating stratiform cloud~~stratiform precipitation~~ around $50\,\mathrm{km}$ south of the coast of Panama (Fig. 2). Radar, lidar and radiometer measurements (Fig. 3) reveal distinct regimes of light, moderate and heavy rain below a melting layer around $4.5\,\mathrm{km}$ above sea level, contiguous with ice clouds with tops between $6 - 10\,\mathrm{km}$. The scene is overlain by cirrus between $10 - 15\,\mathrm{km}$, which is primarily detected by the lidar. In light rain between 15:54 and 15:55 UTC the 94 GHz radar is barely attenuated. Moderate stratiform rain follows from 15:55 and 16:03 UTC, with a strong 9.6 GHz bright band evident, and 94 GHz PIA between 5 and 20 dB. Finally a heavy shower is embedded within the moderate rain between 16:01 and 16:02 UTC. In the latter regime the 94 GHz radar is completely attenuated such that PIA saturates around 60 dB~~65 dB~~; 94 GHz radar reflectivity and mean Doppler velocity measurements are therefore not available within these~~the~~ heaviest rain profiles.

The retrieved variables (Figs. 4a–4e), and forward-modelled 94 GHz and 9.6 GHz radar measurements (Figs. 4f–4j) are compared for the ZvPIA, Zv and ZPIA retrievals. We evaluate the retrievals at a height of $3\,\mathrm{km}$ above sea level, approximately $1\,\mathrm{km}$ below the melting layer.

4.1.1 Moderate rain (15:55–16:01 and 16:02–16:03 UTC)

In the moderate rain regime the ZvPIA retrieval estimates rain rates of $1.0 - 2.0\,\mathrm{mm\,h^{-1}}$ at the melting layer. In profiles with strong attenuation (PIA up to 20 dB), R is close to constant from the melting layer to the surface; conversely, in less attenuated profiles (with PIA around 10 dB) some evaporation is evident, with R reducing to $0.1 - 1.0\,\mathrm{mm\,h^{-1}}$ at the surface (Fig. 4a). Estimates of N_w are consistently between 10^6–$10^7\,\mathrm{m}^{-4}$ in this regime (Fig. 4c), close to the Marshall and Palmer (1948) value, while~~.~~ D_0 is around $1.0\,\mathrm{mm}$ at the melting layer and decreases~~, reducing~~ somewhat toward the surface in profiles where evaporation is strong (Fig. 4d). Forward-modelled 94 GHz radar measurements agree with observations at $3\,\mathrm{km}$ (Figs. 4f–h), as expected since the retrieval minimizes differences between the observed and forward-modelled variables. ~~Comparisons of the independent~~ 9.6 GHz radar measurements ~~with those~~ forward-modelled from the retrieved state show generally good agreement with independent observations at $3\,\mathrm{km}$ above sea level (Figs. 4i and 4j), although 9.6 GHz radar reflectivity is overestimated by as much as 3 dB in profiles with strong evaporation between 15:58 and 16:00 UTC, and mean Doppler velocity is underestimated in the profiles with the heaviest rain. ~~Moderate rain profiles with significant evaporation are well-represented by the ZvPIA retrieval, however these profiles correspond to the strongest differences compared to the independent 9.6 GHz radar reflectivity.~~

The averaged vertical profiles of the ZvPIA retrieval in moderate rain (Fig. 5), show that the forward-modelled 94 GHz radar reflectivity is over-estimated near the surface, while the largest error in 9.6 GHz is in the mean Doppler velocity in the lowest 2 – 3 km. We suggest that these errors in the forward-modelled variables through the vertical profile relate to the representation of N_w as constant with height, such that the effects of evaporation on the DSD—a decrease in concentration of the smallest drops—is not resolved. In a vertically-averaged sense, however, the ZvPIA retrieval is broadly able to reproduce the 9.6 GHz radar reflectivity, while slightly under-estimating mean Doppler velocity.

~~We use the~~ The ZPIA and Zv retrievals ~~of R-N_w~~ illustrate~~to demonstrate~~ the contributions of mean Doppler velocity and PIA to a ZvPIA~~successful~~ retrieval, and the ambiguities that arise in under-constrained retrievals. Both ZPIA and Zv retrievals are considerably more sensitive to the selection of priors and uncertainties than the ZvPIA retrieval. At 3 km above sea level (Fig. 4), ZPIA estimates of R in the moderate rain regime are close to those of ZvPIA, but N_w and D_0 differ significantly, with ZPIA estimating a much higher concentration of smaller drops than ZvPIA. Forward-modelled mean Doppler velocity shows that this retrieval leads to large~~significant~~ errors in~~of~~ drop fallspeeds. The Zv retrieval tends to underestimate~~underestimates~~ the rain rate in this regime by up to an order of magnitude, tending toward the prior R of $0.1\,\mathrm{mm\,h^{-1}}$, with the exception of the strongly attenuated profiles 15:57–15:58 UTC where Zv is able to reproduce the observed PIA from the profiles of radar reflectivity and mean Doppler velocity: while D_0 is well constrained by the mean Doppler velocity, without a constraint on PIA~~the total attenuation from PIA,~~ the retrieved drop number concentration and rain rate are~~is~~ lower than that estimated from ZvPIA; the forward-modelled observations confirm~~s~~ that the Zv retrieval meets reflectivity and mean Doppler velocity constraints, but tends to~~ward~~ represent~~ing~~ weakly-attenuating profiles of rain; the forward-modelled 9.6 GHz variables~~measurements~~ show that this retrieval leads to a significantly under-estimated~~ in~~ radar reflectivity at this frequency~~the unattenuated wavelength~~.

~~Selected profiles of retrieved and forward-modelled variables at 15:58:00 UTC (Fig. 5) illustrate how the Zv and ZPIA retrievals differ from ZvPIA through the vertical profile. With constraints on PIA, both ZPIA and ZvPIA retrievals estimate profiles of R that are close to constant with height; without a Doppler constraint on drop size, the ZPIA retrieval represents the observed PIA with a higher number of smaller drops than the ZvPIA retrieval, leading to a mean Doppler velocity around $1.0\,\mathrm{m\,s^{-1}}$ lower than observed. Conversely, the Zv retrieval has a strong constraint on drop size and therefore forward-modelled mean Doppler velocity, but without a constraint on PIA N_w is underestimated~~~~a low concentration of drops is estimated, with R and D_0 decreasing toward the surface.~~

4.1.2 Light rain (15:54–15:55 UTC)

In the light rain regime, ZvPIA estimates R in the range $0.002 - 0.1\,\mathrm{mm\,h^{-1}}$ and N_w in the range $10^5 - 10^6\,\mathrm{m^{-4}}$. The lower rain rate corresponds to an observed $1.0\,\mathrm{m\,s^{-1}}$ decrease in 94 GHz mean Doppler velocity compared to the moderate rain regime; the retrieval resolves smaller drops in the light rain, with D_0 around 0.5 mm. The forward-modelled 9.6 GHz radar measurements from the ZvPIA retrieval are consistent with independent observations.

Zv retrieves R consistent with ZvPIA throughout the light rain regime, while ZPIA somewhat overestimates R in these profiles. PIA is negligible and therefore provides little additional information in this regime: therefore the ZPIA retrieval represents a higher concentration of smaller drops as the retrieved R and N_w tend~~s~~ to the priors. This sensitivity to the prior when observational information is limited was demonstrated in Section 3 and, as in that synthetic case, the ZPIA retrieval here could be improved with a more appropriate prior. In contrast, with Doppler velocity information to constraint drop size and PIA negligible, the DSD retrieved by Zv is very close to that of ZvPIA. The strong performance of Zv in light rain suggests ~~strong~~ potential for using Doppler radar for R-N_w retrievals of light rain over land.

4.1.3 Heavy shower (16:01–16:02 UTC)

The upper limit of the $94\,\mathrm{GHz}$ radar frequency for rain retrievals is reached in the heavy shower, where PIA is saturated and no radar reflectivity or Doppler information is available below the melting layer. Based on the saturated PIA and the gradient of radar reflectivity in the first few gates, both ZvPIA and ZPIA retrievals estimate R up to $10\,\mathrm{mm\,h^{-1}}$; large uncertainties in R reflect the dearth of information available for retrievals in these profiles, however the $9.6\,\mathrm{GHz}$ radar measurements are broadly consistent with profiles in which ZPIA and ZvPIA estimate rain rates around $10\,\mathrm{mm\,h^{-1}}$. Without PIA information, the Zv retrieval interprets the deficit in radar reflectivity as a drop in rain rate and drop size, and adds significant uncertainty to the retrieved quantities. The estimates of N_w vary over many orders of magnitude and are clearly unconstrained by observations in this regime; the R-N_w retrieval is not warranted without sufficient observational information, however PIA does appear to be sufficient for to estimate R, with increased uncertainty.

In this case of tropical stratiform rain the $94\,\mathrm{GHz}$ radar is fully attenuated by rain rates around $10\,\mathrm{mm\,h^{-1}}$ falling from a melting layer around $4.0\,\mathrm{km}$ above sea level. In the midlatitudes, however, where melting layers are much shallower, successful R-N_w retrievals should be possible up to higher rain rates before the radar is fully attenuated.

4.1.4 Joint frequencies of retrieved and forward-modelled variables

A more comprehensive evaluation of the retrievals against independent $9.6\,\mathrm{GHz}$ radar measurements can be made using the joint frequencies of retrieved state variables (Figs. 6a–6c) and forward-modelled $9.6\,\mathrm{GHz}$ radar measurements (Figs. 6d–6f) for each retrieval. The major modes in the rain retrieval are evident in the distributions of R and N_w relative to the priors (dashed lines), and in the distribution of $9.6\,\mathrm{GHz}$ radar reflectivity and mean Doppler velocity compared against observations (black contours). In the $9.6\,\mathrm{GHz}$ radar variables the moderate rain regime exhibits radar reflectivity around $20\,\mathrm{dBZ}$ and mean Doppler velocity between $6-7\,\mathrm{m\,s^{-1}}$, while the light rain regime has radar reflectivity between $0-5\,\mathrm{dBZ}$ and mean Doppler velocity around $3\,\mathrm{m\,s^{-1}}$.

The ZPIA retrieval has a dominant mode corresponding to the moderate rain regime, with R between $0.5-2.0\,\mathrm{mm\,h^{-1}}$ and a higher N_w with respect to the prior; without a constraint on mean Doppler velocity this retrieval represents a relatively high concentration of small drops. The corresponding forward-modelled measurements shows the small drop size leads to a significant underestimate of both mean Doppler velocity and radar reflectivity at $9.6\,\mathrm{GHz}$.

Without a PIA constraint~~PIA information to constraint the total attenuation in the profile~~, Zv retrievals in the moderate rain regime tend toward weakly attenuated profiles with N_w less than $10^6\,\mathrm{m^{-4}}$, where R is close to~~tends toward~~ the prior. This leads to underestimates of radar reflectivity by more than $10\,\mathrm{dB}$; the mean Doppler velocity is reasonably well-constrained, but broadly underestimated by around $1\,\mathrm{m\,s^{-1}}$. A secondary mode with N_w close to the prior and R greater than $1\,\mathrm{mm\,h^{-1}}$ represents the strongly attenuated profiles of moderate rain in which Zv comes close to reproducing the observed PIA. Light rain profiles are represented with $N_w \approx 10^6\,\mathrm{m^{-4}}$, somewhat overestimating mean Doppler velocity.

ZvPIA resolves distinct modes for light and moderate rain regimes in the retrieved variables, and each mode corresponds well to the observed $9.6\,\mathrm{GHz}$ radar measurements: the moderate rain regime is represented with heavier rain than the Zv retrieval, but with a lower concentration of smaller drops than the ZPIA retrieval; the light rain regime is similar to that of the Zv retrieval, where the negligible PIA provides little additional information. Both rain regimes have N_w around $10^6\,\mathrm{m^{-4}}$, consistent with the average value of $2 \times 10^6\,\mathrm{m^{-4}}$ for stratiform rain found by Testud et al. (2001). The $9.6\,\mathrm{GHz}$ radar reflectivity is well-represented across both rain regimes, however the mean Doppler velocity shows that drop fallspeed is slightly under-estimated in moderate rain, and over-estimated in the light rain; this may be due to the retrieval assuming N_w is constant with height in each profile, such that any variations in the DSD with height are expressed as changes in drop size, rather than in drop number concentration.

We~~In summary, we~~ have retrieved R as a function of both D_0 and N_w for a case of stratiform rain from melting ice,including ~~across~~ rain rates ~~varying~~ from light rain as low as $10^{-3}\,\mathrm{mm\,h^{-1}}$, to a heavy shower with R up to $10\,\mathrm{mm\,h^{-1}}$. The retrieved N_w was around $10^6\,\mathrm{m^{-4}}$ throughout the case, which is consistent with expectations for average drop number concentrations in this context; the exception is in the heavy rain shower where the $94\,\mathrm{GHz}$ radar becomes fully attenuated, and insufficient information is available for a R-N_w retrieval. The Zv retrieval, an analogue for Doppler radar retrievals over land, performed very well in light rain where total attenuation is close to zero, but tended towards the R prior in profiles of moderate~~moderate rain profiles~~ where attenuation makes radar reflectivity ambiguous, and R tends to be under-estimated. ZPIA retrievals without mean Doppler velocity information tend to estimate R broadly accurately, but retrieve DSDs with a high ~~number~~ concentration of small drops, leading to errors with respect to the independent radar measurements; indeed, since the estimated N_w were close to expectations in this context, a good non-Doppler retrieval of R could have been made by assuming the value of N_w is equal to the prior.

4.2 Case 2: evaporating rain from melting ice, 22 July 2007

We now evaluate the R-N_w retrieval for a case of very light rain from melting ice~~very light rain falling from ice,~~ much of which evaporates before reaching the ground. ER-2 overflew a $60\,\mathrm{km}$ section of stratiform~~ice~~ cloud $300\,\mathrm{km}$ south of Costa Rica, between 13:12~~:00~~–13:17~~:30~~ UTC on 22 July 2007. Light rain was observed below ~~ice~~ clouds with tops between $10-12\,\mathrm{km}$ (Fig. 7). Below the melting layer both $94\,\mathrm{GHz}$ and $9.6\,\mathrm{GHz}$ radar reflectivity are less than $10\,\mathrm{dBZ}$ and decrease~~decreasing~~ toward the surface; the exception is a region of higher $9.6\,\mathrm{GHz}$ radar reflectivity between 13:16–13:17 UTC, ~~and~~ $94\,\mathrm{GHz}$

PIA is small but non-zero~~negligible~~, around 3 dB. In combination with low 94 GHz PIA, the observations suggest significant evaporation~~stratiform light rain evaporating~~ in the lower atmosphere, including ~~significant~~ virga.

Time series of retrieved variables (Figs. 8a and 8e), and forward-modelled 94 GHz and 9.6 GHz radar measurements (Figs. 8f and 8j) are evaluated against observations. We compare ZPIA, Zv and ZvPIA retrievals at a height of 4 km above sea level, which is just below the melting layer.

ZvPIA makes a consistent representation~~retrieval~~ of evaporating light stratiform rain, with R between $0.1-0.2\,\mathrm{mm\,h^{-1}}$ at the melting layer, down to a minimum detectable rate of $10^{-3}\,\mathrm{mm\,h^{-1}}$ ~~near the surface~~ or at the limits of the virga. In the heaviest rain profiles between 13:16–13:17, R is around $0.1\,\mathrm{mm\,h^{-1}}$ at the surface, with D_0 as large as $1.5\,\mathrm{mm}$. Retrieved N_w is consistently around $10^5\,\mathrm{m^{-4}}$, an order of magnitude lower than the previous case of stratiform rain from melting ice, and significantly lower than the prior. Forward-modelled 9.6 GHz radar variables shows ~~very~~ good agreement with independent measurements 4 km;~~, which can be expected as there should be little ambiguity in the retrieval due to attenuation.~~ however, the averaged vertical profiles (Fig 9) show that, while the vertical profile of 94 GHz variables are well-represented, 9.6 GHz radar reflectivity is strongly underestimated in the lowest 3 km. We suggest that these errors in the vertical distribution are due to the effects of evaporation on the DSD, which are not fully resolved in this retrieval of N_w as constant with height: we would expect N_w to decrease toward the surface as the smallest drops evaporate, while errors in forward-modelled mean Doppler velocity at both radar frequencies suggest the raindrop size may be underestimated near the surface.

Similar to the light rain profiles of Case 1, both ZPIA and Zv retrievals make estimates of R close to the ZvPIA retrieval. ZPIA retrievals slightly overestimates R with N_w again close to the prior, which is 2 to 3 orders of magnitude higher than ZvPIA estimates; the corresponding low D_0 of around $0.5\,\mathrm{mm}$ leads to significant differences between forward-modelled and observed mean Doppler velocities. Zv estimates of D_0 are well-constrained by mean Doppler velocity, and where PIA is negligible the Zv retrieval is identical to that of ZvPIA. As noted in the previous case, this indicates that it may~~should~~ be possible to make a~~n accurate~~ R-N_w retrieval of light rain over land with Doppler radar.

4.3 Case 3: warm rain from liquid clouds, 29 July 2007

In warm rain from liquid clouds we expect a distinct DSD with a higher concentration of smaller drops, and with drop growth between cloud-top and the surface (Lebsock et al., 2011). On 29 July 2007 ER-2 overflew a 120 km section of precipitating warm marine cloud around 500 km south of Costa Rica between 12:41–12:51 UTC (Fig. 10). In the first part of the flight (12:41–12:46~~5~~ UTC) observations suggest moderate rainfall corresponding to deeper cloud tops around 3.5 km: PIA varies between $10-50$ dB in narrow features, where 9.6 GHz radar reflectivity exceeds 20 dBZ. The following section (12:46~~5~~–12:51 UTC) is characterised by shallower stratiform cloud with tops around 3 km, and is associated with patchy light precipitation and~~with~~ PIA between $0-10$ dB.

Concurrent to the rain retrieval shown here, we use the lidar to retrieve liquid cloud, which also contributes to the attenuation of 94 GHz radar. The retrieved properties of the liquid cloud do not vary between the different retrievals compared here, and we do not evaluate the retrieval of cloud liquid water content in this study; however, as discussed in Section 2.2, lidar is quickly extinguished at cloud-top and radar is most sensitive to drizzle drops, so that cloud base is rarely known in the target classification.Hence we~~we~~ acknowledge that the simultaneous retrieval of cloud and precipitation in warm clouds from 94 GHz radar is a source of uncertainty that warrants further consideration (e.g. Haynes et al., 2009; Hawkness-Smith, 2010; Mace et al., 2016).

The retrieved variables (Fig.11a–11e) and forward-modelled radar measurements (Fig.11f–11j) are compared at 1 km above sea level, and compared against 94 GHz and 9.6 GHz radar measurements. We compare ZPIA, Zv and ZvPIA retrievals as in the previous cases. Warm rain or drizzle forming ~~from collision and coalescence~~ in liquid clouds can be easily distinguished from rain falling below ice clouds within the target classification scheme, so that physically appropriate choices for the priors and the physical representations of state variables can be configured in CAPTIVATE for distinct warm and “cold” rain regimes; however, in this study we use the same prior R and N_w throughout.

4.3.1 Moderate rain (12:41–12:46~~5~~ UTC)

The ZvPIA retrieval resolves a strong increase in~~of~~ rain rate from cloud-top, where R is between $0.1-1.0\,\mathrm{mm\,h^{-1}}$, to the surface, where R increases to $1.0-10.0\,\mathrm{mm\,h^{-1}}$. Retrieved N_w is consistently around $10^{10}\,\mathrm{m^{-4}}$ in the moderate rain regime, several orders of magnitude greater than were estimated for~~retrieved for~~ rain from melting ice; accordingly, the drops~~the corresponding drop sizes~~ are much smaller, with D_0 increasing from $0.1-0.3\,\mathrm{mm}$ at cloud-top~~,~~ to $0.2-0.5\,\mathrm{mm}$ near the surface. At 1 km above sea level t~~T~~he 94 GHz radar measurements correspond very well to the forward-modelled variables.~~,~~ The~~and the~~ 9.6 GHz radar reflectivity is also ~~exceptionally~~ close to the forward-model~~; this is because at the small drop sizes in this context scattering is in the Rayleigh regime for both radar frequencies~~; however, while the~~. The~~ forward-modelled mean Doppler velocity at 9.6 GHz also tracks well with observations, peaks associated with the heaviest precipitation features are not resolved.

The vertical structure of 94 GHz and 9.6 GHz radar reflectivity is well represented in the ZvPIA retrieval over the moderate warm rain regime (Fig 12); however, mean Doppler velocity is under-estimated by around $1\,\mathrm{m\,s^{-1}}$ in the lowest 1 km at both radar frequencies. The retrieval of constant-N_w for each profile allows a broadly satisfactory retrieval of the rain DSD with a good fit to observations, but evaluation of the full vertical profiles shows that some microphysical process is not resolved: in warm rain we expect collision and coalescence to lead to both an increase in drop size and a decrease in drop number concentration toward the surface. It seems likely, as for the representation of evaporation in case 2, that while the retrieval of N_w allows for an improved retrieval of the DSD across a range of rain regimes, there are limits to the vertical variability of the DSD that can be resolved with a height-invariant N_w.

The~~At 1 km the~~ ZPIA retrieval closely~~strongly~~ resembles ZvPIA; this includes matching estimates of D_0, despite having no constraint on drop size from mean Doppler velocity. ~~The forward-modelled 94 GHz and 9.6 GHz mean Doppler velocities for the ZPIA retrieval are very close to observations.~~ Zv retrieves similar D_0~~In contrast, Zv also retrieves D_0 correctly~~, but frequently under-estimates N_w by as much as 2 orders of magnitude: the Zv-retrieved DSD has fewer drops and negligible PIA at 94 GHz, which corresponds to very large errors in forward-modelled 9.6 GHz radar reflectivity. Unlike the stratiform rain cases, here PIA is more important for an accurate retrieval than mean Doppler velocity: the mean Doppler velocity may be~~is~~ less sensitive to the changes in terminal fallspeed due to variations in the sizes of small drops, while PIA in combination with radar reflectivity provide an effective constraint on the number concentration because only a DSD with many small drops satisfies the observed strong attenuation and low radar reflectivity.

4.3.2 Light rain (12:46–12:51 UTC)

In the light warm rain ZvPIA estimates patchy precipitation features with R between $0.01 - 0.5\,\mathrm{mm\,h^{-1}}$ and median drop sizes around $0.1 - 0.3\,\mathrm{mm\,h^{-1}}$, similar to values at the tops of the deeper warm clouds, but without significant drop growth toward the surface. The retrieved N_w in the lightest rain profiles is around $10^8 - 10^9\,\mathrm{m^{-4}}$, but returns to $10^{10}\,\mathrm{m^{-4}}$ where heavier rain features are evident. The forward-modelled radar reflectivities are close to observations at $1\,\mathrm{km}$, while the mean Doppler velocity again matches the lower range of measurements, but not the ~~noisy~~ peaks. ~~The forward-modelled PIA is $0\,\mathrm{dB}$ in the lightest rain profiles, while measurements indicate non-zero attenuation of around $1 - 3\,\mathrm{dB}$.~~ ZPIA estimates R similar to ZvPIA in the stratus regime, but without a Doppler velocity constraint in the lightest profiles, ZPIA retrieves fewer, larger drops, with N_w tending toward the prior at $8 \times 10^6\,\mathrm{m^{-4}}$. In contrast, Zv is very similar to ZvPIA in the lightest profiles~~rain~~.

In warm rain, we have retrieved~~In summary, it is possible to retrieve~~ N_w several orders of magnitude greater than the Marshall–Palmer value, with D_0 in the range $0.1 - 0.5\,\mathrm{mm}$ in rain rates~~across a range of R~~ from very light drizzle~~,~~ up to $10\,\mathrm{mm\,h^{-1}}$ in the heaviest profiles~~ of warm rain from liquid clouds~~. The contribution of PIA and mean Doppler velocity to R-N_w retrievals in warm rain differs from that in rain from melting ice: while Doppler is required to retrieve N_w when attenuation is low, it is possible to retrieve N_w without Doppler in strongly attenuated profiles of warm cloud, where the combination of low radar reflectivity and high attenuation can only be due to a high concentration of small drops.

5 Dual-frequency radar retrievals

ER-2 aircraft measurements from TC4 provide a rare opportunity for airborne observations with multiple Doppler radars. In this study we have primarily used the $9.6\,\mathrm{GHz}$ radar to evaluate retrievals made with the $94\,\mathrm{GHz}$ radar; however, we can also use the dual-frequency radar measurements to exploit the different scattering behaviours and retrieve additional information about the DSD. Dual-frequency ratio (DFR) and differential Doppler velocity (DDV) techniques have been applied to retrievals from ER-2 measurements during the CRYSTAL-FACE field experiment over Florida in 2002 (Liao et al., 2008, 2009), and Tian et al. (2007) exploited dual-frequency Doppler radar to retrieve rain DSD and vertical air motion for light stratiform rain from the same experiment. The CAPTIVATE framework can combine information from two radars, resolving differential non-Rayleigh scattering and mean Doppler velocities from multiple wavelengths.

We compare the~~The~~ dual-frequency radar retrievals, with and without mean Doppler velocity measurements~~, are compared~~ against the ZvPIA $94\,\mathrm{GHz}$ retrieval for Case 1 ~~on 22 July 2007~~, which covered a wide range of rain intensities, including a region in which the $94\,\mathrm{GHz}$ radar was fully attenuated (Fig. 13). The dual-frequency radar retrieval estimates of R are consistent with those from $94\,\mathrm{GHz}$ ~~retrievals~~, with the exception of the non-Doppler dual-frequency radar retrieval in ~~the~~ light rain, where a high concentration of small drops is estimated, leading to an over-estimate of R; in much of the lightest rain ~~profiles~~ the hydrometeors may be below the sensitivity of the 9.6 GHz instrument, so that the dual-frequency radar retrieval tends toward that ~~of the ZPIA retrieval~~ from the 94 GHz radar. In the heavy shower, where the ZvPIA estimates of Z have large uncertainties and N_w is very poorly constrained due to complete extinction of the 94 GHz radar beam, the dual-frequency radar retrievals use ~~the unattenuated~~ 9.6 GHz measurements alone to estimate R around $10\,\mathrm{mm\,h^{-1}}$; N_w remains in the range $10^6 - 10^7\,\mathrm{m^{-4}}$ as in the surrounding moderate rain, and D_0 is estimated between $1-2\,\mathrm{mm}$. This illustrates~~confirms~~ that the 94 GHz retrieval was capable of a cautious estimate of R with large retrieval uncertainty, based on the gradient of radar reflectivity and saturated PIA; however, ~~ZvPIA~~ estimates of N_w cannot be~~by~~ justified when the radar is fully attenuated. The greatest errors in the non-Doppler dual-frequency radar retrieval are in forward-modelled Doppler velocity for the evaporating moderate rain profiles between 15:58–16:00 UTC, where a higher concentration of smaller drops is retrieved; in this circumstance the addition of Doppler velocity information leads to a stronger retrieval than a second radar wavelength. Overall the close agreement of the 94 GHz Doppler radar retrievals with the dual-frequency Doppler retrieval is a promising result, indicating that a single frequency Doppler radar is sufficient for a retrieval of R and N_w within the limits of radar attenuation.

6 Retrieving vertical profiles of N_w

We have demonstrated the retrieval of rain rate as a function of both D_0 and N_w, making the simplifying assumption that N_w is constant with height in each profile. We argue that this is a significant improvement over retrievals in which N_w is assumed constant everywhere, and have retrieved values of N_w ranging over more than five orders of magnitude between light rain from melting ice and warm rain from liquid clouds; however, evaluation against 9.6 GHz radar measurements showed that features within the vertical profile are not always accurately resolved, with the most significant errors near the surface in cases where microphysical processes are expected to affect the DSD with height.

It is of interest to represent changes in N_w through the vertical profile; however, there are limits to the degrees of freedom that can be retrieved with the available observed variables. In this section we explore the potential for one additional degree of freedom, by allowing each profile of N_w to be represented by a linear gradient, as as explored in Rose and Chandrasekar (2006) for a dual-frequency retrieval. Here the state vector becomes:

$$\mathbf{x} = \ln \left[R_1 \cdots R_n \quad \overline{N_w} \quad {N_w}' \right]^{\mathrm{T}} \tag{12}$$

where $\overline{N_w}$ is the average N_w through the profile and ${N_w}'$ is the gradient with height.

A retrieval in which N_w is represented by a linear profile ("linear-N_w") is compared against the "constant-N_w" ZvPIA retrieval, using the average profiles of retrieved and forward-modelled variables for a ZvPIA retrieval of moderate warm rain from Case 3 (Fig. 14). The linear-N_w retrieval significantly improves the fit with 94 GHz observed variables below 1.5 km, where the constant-N_w retrieval underestimates mean Doppler velocity and overestimates radar reflectivity. The linear-N_w retrieval is also better able to forward-model the independent 9.6 GHz radar variables, with near-surface errors in mean Doppler velocity significantly reduced. The linear-N_w retrieval resolves a gradient in N_w from around $10^{11}\,\mathrm{m^{-4}}$ at cloud-top to $10^9\,\mathrm{m^{-4}}$

near the surface, and a steeper gradient of D_0, with corresponding drop size increasing from almost $0.1\,\mathrm{mm}$ near cloud-tops to around $0.5\,\mathrm{mm}$ at the surface. The changes in D_0 and N_w through the vertical profile have relatively minor effects on the profile-averaged rain rate, with the retrieved R increasing somewhat above $2\,\mathrm{km}$, and a decreasing below $0.5\,\mathrm{km}$ by around a factor of 2.

With an additional degree of freedom, the linear-N_w retrieval from $94\,\mathrm{GHz}$ radar exhibited increased temporal variability between profiles of the retrieved variables; however, a dual-frequency retrieval (as in Section 5) including a linear representation of N_w estimated substantially similar profiles of N_w and D_0 for this case, indicating that the retrieved profiles are robust when better constrained by additional observations. The retrieval of a linear gradient N_w leads to an improved representation of the vertical profile, both as evaluated against independent $9.6\,\mathrm{GHz}$ radar variables, and in that the retrieved profiles of N_w and D_0 qualitatively meet expectations for collision and coalescence processes in warm rain. Nevertheless, we note that the profile-averaged N_w is close to that retrieved with a height-invariant N_w, and that the corresponding changes in retrieved R are small in a vertically-averaged sense.

7 Discussion and conclusions

The upcoming ESA/JAXA EarthCARE satellite will include a~~the~~ $94\,\mathrm{GHz}$ cloud profiling radar, the first Doppler radar in space. In this study we have used airborne Doppler radar~~aircraft~~ measurements to investigate the prospects for improved ~~global~~ rain retrievals from a spaceborne Doppler radar, with a focus on improving~~how mean Doppler velocity measurements stand to improve~~ upon $94\,\mathrm{GHz}$ radar rain retrievals from CloudSat in two key respects: (1) to facilitate rain rate estimates over land, and; (2) to reduce uncertainties in rain rate estimates by retrieving an additional parameter of the raindrop size distribution (DSD). Retrievals over a range of stratiform rain regimes were made using measurements from the $94\,\mathrm{GHz}$ Doppler radar aboard the ER-2 aircraft during the TC4 field campaign over the tropical Pacific in 2007, and evaluated against independent measurements from a less attenuated $9.6\,\mathrm{GHz}$ Doppler radar.~~second Doppler radar at a less an unattenuated wavelength~~.

The CAPTIVATE algorithm has been developed for rain, cloud and aerosols retrievals from the synergy of active and passive instruments; within the variational scheme, multiple observational variables can be combined as available, and the retrieved variables and their physical representation can be configured at runtime. It is therefore possible with CAPTIVATE to combine the information from multiple radar measurements, and to estimate uncertainties in retrieved variables propagated from uncertainties in the observations and forward-models.

We have shown that the ambiguities of rain rate retrievals at strongly~~from~~ attenuated radar frequencies can be resolved by either an estimate of path-integrated attenuation (PIA)~~PIA~~ or by the profile of mean Doppler velocity, a measure of drop terminal fallspeed relating to drop size, and which is not affected by partial attenuation of the radar beam.~~mean Doppler velocity measurements.~~ The latter has~~, with the latter having~~ potential applications to making estimates of rain rate over land , where PIA is more difficult to estimate from the surface backscatter. Furthermore, information from both PIA and mean Doppler velocity can be used to retrieve the rain rate as a function of both median drop size D_0 and drop number concentration N_w, improving upon significant uncertainties in rain rate estimates owing to assumptions about the DSD.

Retrievals of rain rate R and drop number concentration N_w using combined radar reflectivity, PIA and mean Doppler velocity measurements from~~from the~~ $94\,\mathrm{GHz}$ radar were evaluated over three cases of tropical stratiform rain over the ocean. The selected cases covered a range of rain rates from virga to heavy showers from~~rain from both~~ melting ice and liquid clouds. The $94\,\mathrm{GHz}$ radar was fully attenuated in profiles with~~by~~ rain rates around $10\,\mathrm{mm\,h^{-1}}$ ~~falling~~ below a melting layer above $4\,\mathrm{km}$, and in rain from~~in slightly heavier rain rates from~~ liquid clouds with tops around $3\,\mathrm{km}$. The attenuation of the $94\,\mathrm{GHz}$ radar places an upper limit on the rain profiles that can be retrieved; however, in the mid-latitudes where the melting layer is lower, it may be possible to make retrieval up to higher rain rates before the radar is fully attenuated. The $9.6\,\mathrm{GHz}$ radar wavelength was subsequently used~~included~~ to make a dual-frequency radar retrieval (Section 5). In profiles where the $94\,\mathrm{GHz}$ was fully attenuated, the dual-frequency estimates of rain rate were consistent with those derived from the gradient of $94\,\mathrm{GHz}$ radar reflectivity. Retrieved values of N_w ranged from $10^5\,\mathrm{m^{-4}}$ in light rain from melting ice, with D_0 around $1.0-1.5\,\mathrm{mm}$, up to N_w of $10^{10}\,\mathrm{m^{-4}}$ in moderate rain from liquid cloud, where D_0 was around $0.1-0.3\,\mathrm{mm}$.

In many contexts collision–coalescence, evaporation and breakup processes are expected to modify the DSD through the vertical profile. With N_w retrieved as constant with height the retrieval was broadly able to represent the major features of the vertical profile when evaluated against independent $9.6\,\mathrm{GHz}$ radar measurements, but errors in the gradient of mean Doppler velocity suggested that the effects of evaporation or collision–coalescence on the DSD through the profile were not resolved. We demonstrated that the $94\,\mathrm{GHz}$ radar measurements, including both mean Doppler velocity and PIA, are sufficient to retrieve a more complex representation of N_w with height (Section 6): in warm rain from liquid cloud it was possible to resolve the decrease in drop concentration and increase in drop size toward the surface consistent with collision–coalescence, while improving on errors with respect to forward-modelled $9.6\,\mathrm{GHz}$ radar measurements. The retrieval of a vertical gradient of N_w has potential applications to both single- and multiple-frequency retrievals of precipitation (e.g. Rose and Chandrasekar, 2006), but must be constrained by sufficient observational variables.

~~Mean Doppler velocity provides a strong constraint on D_0 that is not compromised by partial attenuation of the radar beam. In combination with radar reflectivity, mean Doppler velocity is sufficient to resolve the ambiguities of radar reflectivity profiles due to attenuation, supporting retrievals of rain rate over land where PIA cannot be estimated from the surface reference technique.~~ In~~Furthermore, in~~ combination with PIA, the Doppler velocity information provided sufficient information to make robust retrievals of R-N_w across a range of rain regimes. In light rain with negligible PIA, Doppler velocity is sufficient to retrieve R and N_w, suggesting the possibility of using~~for~~ Doppler radar for R-N_w retrievals of light rain over land without PIA; however, in moderate rain rates PIA is necessary to constrain the retrieval. Satisfactory retrievals of rain rate may be made over land by assuming N_w constant, especially for stratiform precipitation, or PIA could be estimated from the land surface backscatter with a large observational uncertainty (as in Iguchi et al., 2009), which may provide sufficient information to resolve the ambiguity between weakly and strongly attenuating profiles. A robust method of using Doppler radar to estimating rain rate over land will be the subject of future work.

With a constraint on PIA, the gradient of apparent radar reflectivity can be used to estimate R. While Doppler velocity is generally required to retrieve N_w, in moderate warm rain from liquid clouds the combination of low radar reflectivity and strong attenuation was sufficient to retrieve the high concentration of small drops typical of warm rain, without the need for Doppler velocity information: this finding may be applicable to retrievals of the drop number concentration in warm rain observed by CloudSat.

We have demonstrated the contribution of mean Doppler velocity to assimilating drop size information in estimates of rain rate. With the first Doppler radar in space, EarthCARE synergy retrievals will exploit novel measurements to improve the~~EarthCARE will make a significant contribution to the~~ satellite remote sensing of clouds and precipitation~~rain~~. ~~Mean Doppler velocity provides an effective constraint on drop size that can be exploited to estimate rain rate over land, and to reduce uncertainty in rain rate estimates through the vertical profile by retrieving the drop number concentration N_w of the rain DSD, which must otherwise be assumed.~~ Future work will focus on understanding the application of these retrievals to spaceborne Doppler radar, including the effects of multiple scattering and non-uniform beam filling on the Doppler measurements. As part of EarthCARE radar–lidar–radiometer synergy retrievals, improved global estimates of rain rate and drop size ~~from Doppler radar~~ will provide new insights into the interactions of clouds~~, aerosols~~ and precipitation through the atmospheric profile.

Acknowledgements. This work was supported by the National Centre for Earth Observation (NCEO) and European Space Agency Grant 4000112030/15/NL/CT, with computing resources provided by the University of Reading. Dr. Tian's research is supported by NASA Precipitation Measurement Mission and Remote Sensing Theory. We thank Gerry Heymsfield and the ER-2 radar engineers for collecting CRS and EDOP data, Dennis Hlavka (NASA-GSFC) for assistance with CPL data, and Stephen Platnick and Howard Tan (NASA-JPL) with MAS/MASTER radiometer data. ERA-Interim data are produced and distributed by ECMWF, and hosted by the Centre for Environmental Data Analysis.

We are grateful to Alain Protat and two anonymous referees for their constructive feedback, and Ross Bannister, Nancy Nichols, Lars Isaksen, Elias Holm and Mike Rennie for helpful discussions.

References

Abel, S. J. and Boutle, I. A.: An improved representation of the raindrop size distribution for single-moment microphysics schemes, Quarterly Journal of the Royal Meteorological Society, 138, 2151–2162, doi:10.1002/qj.1949, 2012.

Atlas, D., Srivastava, R., and Sekhon, R.: Doppler radar characteristics of precipitation at vertical incidence, Reviews of Geophysics, 1973.

Battaglia, A. and Tanelli, S.: DOMUS: DOppler MUltiple-Scattering Simulator, IEEE Transactions on Geoscience and Remote Sensing, 49, 442–450, doi:10.1109/TGRS.2010.2052818, 2011.

Battaglia, A., Ajewole, M. O., and Simmer, C.: Multiple scattering effects due to hydrometeors on precipitation radar systems, Geophysical Research Letters, 32, n/a–n/a, doi:10.1029/2005GL023810, 2005.

Battaglia, A., Ajewole, M. O., and Simmer, C.: Evaluation of radar multiple scattering effects in Cloudsat configuration, Atmospheric Chemistry and Physics, 7, 1719–1730, doi:10.5194/acp-7-1719-2007, 2007.

Beard, K. V.: Terminal Velocity and Shape of Cloud and Precipitation Drops Aloft, Journal of the Atmospheric Sciences, 33, 851–864, doi:10.1175/1520-0469(1976)033<0851:TVASOC>2.0.CO;2, 1976.

Behrangi, A., Lebsock, M., Wong, S., and Lambrigtsen, B.: On the quantification of oceanic rainfall using spaceborne sensors, Journal of Geophysical Research: Atmospheres, 117, doi:10.1029/2012JD017979, 2012.

Berg, W., L'Ecuyer, T., Haynes, J. M., Berg, W., L'Ecuyer, T., and Haynes, J. M.: The Distribution of Rainfall over Oceans from Spaceborne Radars, Journal of Applied Meteorology and Climatology, 49, 535–543, doi:10.1175/2009JAMC2330.1, 2010.

Ceccaldi, M., Delanoë, J., Hogan, R. J., Pounder, N. L., Protat, A., and Pelon, J.: From CloudSat-CALIPSO to EarthCare: Evolution of the DARDAR cloud classification and its comparison to airborne radar-lidar observations, Journal of Geophysical Research: Atmospheres, 118, 7962–7981, doi:10.1002/jgrd.50579, 2013.

Dee, D. P., Uppala, S. M., Simmons, A. J., Berrisford, P., Poli, P., Kobayashi, S., Andrae, U., Balmaseda, M. A., Balsamo, G., Bauer, P., Bechtold, P., Beljaars, A. C. M., van de Berg, L., Bidlot, J., Bormann, N., Delsol, C., Dragani, R., Fuentes, M., Geer, A. J., Haimberger, L., Healy, S. B., Hersbach, H., H\'{o}lm, E. V., Isaksen, L., K\r{a}llberg, P., K\"{o}hler, M., Matricardi, M., McNally, A. P., Monge-Sanz, B. M., Morcrette, J. J., Park, B. K., Peubey, C., de Rosnay, P., Tavolato, C., Th\'{e}paut, J. N., and Vitart, F.: The ERA-Interim reanalysis: configuration and performance of the data assimilation system, Quarterly Journal of the Royal Meteorological Society, 137, 553–597, doi:10.1002/qj.828, 2011.

Firda, J. M., Sekelsky, S. M., McIntosh, R. E., Firda, J. M., Sekelsky, S. M., and McIntosh, R. E.: Application of Dual-Frequency Millimeter-Wave Doppler Spectra for the Retrieval of Drop Size Distributions and Vertical Air Motion in Rain, Journal of Atmospheric and Oceanic Technology, 16, 216–236, doi:10.1175/1520-0426(1999)016<0216:AODFMW>2.0.CO;2, 1999.

Frisch, A. S., Fairall, C. W., and Snider, J. B.: Measurement of Stratus Cloud and Drizzle Parameters in ASTEX with a K α -Band Doppler Radar and a Microwave Radiometer, Journal of the Atmospheric Sciences, 52, 2788–2799, doi:10.1175/1520-0469(1995)052<2788:MOSCAD>2.0.CO;2, 1995.

Hawkness-Smith, L.: A novel retrieval of liquid water path and a evaluation of the representation of drizzle in numerical models, Ph.D. thesis, University of Reading, http://ethos.bl.uk/OrderDetails.do?uin=uk.bl.ethos.533772, 2010.

Haynes, J. M., L'Ecuyer, T. S., Stephens, G. L., Miller, S. D., Mitrescu, C., Wood, N. B., and Tanelli, S.: Rainfall retrieval over the ocean with spaceborne W-band radar, Journal of Geophysical Research, 114, D00A22, doi:10.1029/2008JD009973, 2009.

Haynes, J. M., Jakob, C., Rossow, W. B., Tselioudis, G., and Brown, J. R.: Major Characteristics of Southern Ocean Cloud Regimes and Their Effects on the Energy Budget, Journal of Climate, 24, 5061–5080, doi:10.1175/2011JCLI4052.1, 2011.

Heymsfield, G. M., Bidwell, S. W., Caylor, I. J., Ameen, S., Nicholson, S., Boncyk, W., Miller, L., Vandemark, D., Racette, P. E., and Dod, L. R.: The EDOP Radar System on the High-Altitude NASA ER-2 Aircraft, Journal of Atmospheric and Oceanic Technology, 13, 795–809, doi:10.1175/1520-0426(1996)013<0795:TERSOT>2.0.CO;2, 1996.

Hitschfeld, W. and Bordan, J.: ERRORS INHERENT IN THE RADAR MEASUREMENT OF RAINFALL AT ATTENUATING WAVE-LENGTHS, Journal of Meteorology, 11, 58–67, doi:10.1175/1520-0469(1954)011<0058:EIITRM>2.0.CO;2, 1954.

Hogan, R. J.: A Variational Scheme for Retrieving Rainfall Rate and Hail Reflectivity Fraction from Polarization Radar, Journal of Applied Meteorology and Climatology, 46, 1544–1564, doi:10.1175/JAM2550.1, 2007.

Hogan, R. J.: Fast Lidar and Radar Multiple-Scattering Models. Part I: Small-Angle Scattering Using the Photon Variance–Covariance Method, Journal of the Atmospheric Sciences, 65, 3621–3635, doi:10.1175/2008JAS2642.1, 2008.

Hook, S. J. S., Myers, J. J. J., Thome, K. K. J., Fitzgerald, M., and Kahle, A. B.: The MODIS/ASTER airborne simulator (MASTER) — a new instrument for earth science studies, Remote Sensing of Environment, 76, 93–102, doi:10.1016/S0034-4257(00)00195-4, 2001.

Hou, A. Y., Kakar, R. K., Neeck, S., Azarbarzin, A. A., Kummerow, C. D., Kojima, M., Oki, R., Nakamura, K., Iguchi, T., Hou, A. Y., Kakar, R. K., Neeck, S., Azarbarzin, A. A., Kummerow, C. D., Kojima, M., Oki, R., Nakamura, K., and Iguchi, T.: The Global Precipitation Measurement Mission, Bulletin of the American Meteorological Society, 95, 701–722, doi:10.1175/BAMS-D-13-00164.1, 2014.

Iguchi, T., Kozu, T., Meneghini, R., Awaka, J., Okamoto, K., Iguchi, T., Kozu, T., Meneghini, R., Awaka, J., and Okamoto, K.: Rain-Profiling Algorithm for the TRMM Precipitation Radar, Journal of Applied Meteorology, 39, 2038–2052, doi:10.1175/1520-0450(2001)040<2038:RPAFTT>2.0.CO;2, 2000.

Iguchi, T., Kozu, T., Kwaitkowski, J., Meneghini, R., Awaka, J., and Okamoto, K.: Uncertainties in the Rain Profiling Algorithm for the TRMM Precipitation Radar, Journal of the Meteorological Society of Japan, 87A, 1–30, doi:10.2151/jmsj.87A.1, 2009.

Illingworth, A. J. and Blackman, T. M.: The Need to Represent Raindrop Size Spectra as Normalized Gamma Distributions for the Interpretation of Polarization Radar Observations, Journal of Applied Meteorology, 41, 286–297, doi:10.1175/1520-0450(2002)041<0286:TNTRRS>2.0.CO;2, 2002.

Illingworth, A. J., Barker, H. W., Beljaars, A., Ceccaldi, M., Chepfer, H., Clerbaux, N., Cole, J., Delanoë, J., Domenech, C., Donovan, D. P., Fukuda, S., Hirakata, M., Hogan, R. J., Huenerbein, A., Kollias, P., Kubota, T., Nakajima, T., Nakajima, T. Y., Nishizawa, T., Ohno, Y., Okamoto, H., Oki, R., Sato, K., Satoh, M., Shephard, M. W., Velázquez-Blázquez, A., Wandinger, U., Wehr, T., and van Zadelhoff, G.-J.: The EarthCARE Satellite: The Next Step Forward in Global Measurements of Clouds, Aerosols, Precipitation, and Radiation, Bulletin of the American Meteorological Society, 96, 1311–1332, doi:10.1175/BAMS-D-12-00227.1, 2015.

King, M. D., Menzel, W. P., Grant, P. S., Myers, J. S., Arnold, G. T., Platnick, S. E., Gumley, L. E., Tsay, S.-C., Moeller, C. C., Fitzgerald, M., Brown, K. S., Osterwisch, F. G., King, M. D., Menzel, W. P., Grant, P. S., Myers, J. S., Arnold, G. T., Platnick, S. E., Gumley, L. E., Tsay, S.-C., Moeller, C. C., Fitzgerald, M., Brown, K. S., and Osterwisch, F. G.: Airborne Scanning Spectrometer for Remote Sensing of Cloud, Aerosol, Water Vapor, and Surface Properties, Journal of Atmospheric and Oceanic Technology, 13, 777–794, doi:10.1175/1520-0426(1996)013<0777:ASSFRS>2.0.CO;2, 1996.

Kollias, P., Rémillard, J., Luke, E., and Szyrmer, W.: Cloud radar Doppler spectra in drizzling stratiform clouds: 1. Forward modeling and remote sensing applications, Journal of Geophysical Research, 116, D13 201, doi:10.1029/2010JD015237, 2011a.

Kollias, P., Szyrmer, W., Rémillard, J., and Luke, E.: Cloud radar Doppler spectra in drizzling stratiform clouds: 2. Observations and microphysical modeling of drizzle evolution, Journal of Geophysical Research, 116, D13 203, doi:10.1029/2010JD015238, 2011b.

Kummerow, C., Barnes, W., Kozu, T., Shiue, J., Simpson, J., Kummerow, C., Barnes, W., Kozu, T., Shiue, J., and Simpson, J.: The Tropical Rainfall Measuring Mission (TRMM) Sensor Package, Journal of Atmospheric and Oceanic Technology, 15, 809–817, doi:10.1175/1520-0426(1998)015<0809:TTRMMT>2.0.CO;2, 1998.

Lebsock, M., Morrison, H., and Gettelman, A.: Microphysical implications of cloud-precipitation covariance derived from satellite remote sensing, Journal of Geophysical Research: Atmospheres, 118, 6521–6533, doi:10.1002/jgrd.50347, 2013.

Lebsock, M. D. and L'Ecuyer, T. S.: The retrieval of warm rain from CloudSat, Journal of Geophysical Research: Atmospheres, 116, D20 209, doi:10.1029/2011JD016076, 2011.

Lebsock, M. D., L'Ecuyer, T. S., and Stephens, G. L.: Detecting the Ratio of Rain and Cloud Water in Low-Latitude Shallow Marine Clouds, Journal of Applied Meteorology and Climatology, 50, 419–432, doi:10.1175/2010JAMC2494.1, 2011.

L'Ecuyer, T. S. and Stephens, G. L.: An Estimation-Based Precipitation Retrieval Algorithm for Attenuating Radars, Journal of Applied Meteorology, 41, 272–285, doi:10.1175/1520-0450(2002)041<0272:AEBPRA>2.0.CO;2, 2002.

Li, L., Heymsfield, G. M., Racette, P. E., Tian, L., and Zenker, E.: A 94-GHz Cloud Radar System on a NASA High-Altitude ER-2 Aircraft, Journal of Atmospheric and Oceanic Technology, 21, 1378–1388, doi:10.1175/1520-0426(2004)021<1378:AGCRSO>2.0.CO;2, 2004.

Liao, L., Meneghini, R., Tian, L., and Heymsfield, G. M.: Retrieval of Snow and Rain From Combined X- and W-Band Airborne Radar Measurements, IEEE Transactions on Geoscience and Remote Sensing, 46, 1514–1524, doi:10.1109/TGRS.2008.916079, 2008.

Liao, L., Meneghini, R., Tian, L., and Heymsfield, G. M.: Measurements and Simulations of Nadir-Viewing Radar Returns from the Melting Layer at X and W Bands, Journal of Applied Meteorology and Climatology, 48, 2215–2226, doi:10.1175/2009JAMC2033.1, 2009.

Liebe, H. J.: An updated model for millimeter wave propagation in moist air, Radio Science, 20, 1069–1089, 1985.

Luke, E. P. and Kollias, P.: Separating Cloud and Drizzle Radar Moments during Precipitation Onset Using Doppler Spectra, Journal of Atmospheric and Oceanic Technology, 30, 1656–1671, doi:10.1175/JTECH-D-11-00195.1, 2013.

Mace, G. G., Avey, S., Cooper, S., Lebsock, M., Tanelli, S., and Dobrowalski, G.: Retrieving co-occurring cloud and precipitation properties of warm marine boundary layer clouds with A-Train data, Journal of Geophysical Research: Atmospheres, 121, 4008–4033, doi:10.1002/2015JD023681, 2016.

Marshall, J. and Palmer, W.: The distribution of raindrops with size, Journal of meteorology, 1948.

Matrosov, S.: Assessment of Radar Signal Attenuation Caused by the Melting Hydrometeor Layer, IEEE Transactions on Geoscience and Remote Sensing, 46, 1039–1047, doi:10.1109/TGRS.2008.915757, 2008.

Matrosov, S. Y.: Potential for attenuation-based estimations of rainfall rate from CloudSat, Geophysical Research Letters, 34, L05 817, doi:10.1029/2006GL029161, 2007.

McGill, M., Hlavka, D., Hart, W., Scott, V. S., Spinhirne, J., and Schmid, B.: Cloud Physics Lidar: instrument description and initial measurement results, Applied Optics, 41, 3725, doi:10.1364/AO.41.003725, 2002.

McGill, M. J.: Combined lidar-radar remote sensing: Initial results from CRYSTAL-FACE, Journal of Geophysical Research, 109, D07 203, doi:10.1029/2003JD004030, 2004.

Meneghini, R. and Liao, L.: Effective Dielectric Constants of Mixed-Phase Hydrometeors, Journal of Atmospheric and Oceanic Technology, 17, 628–640, doi:10.1175/1520-0426(2000)017<0628:EDCOMP>2.0.CO;2, 2000.

Meneghini, R., Eckerman, J., and Atlas, D.: Determination of Rain Rate from a Spaceborne Radar Using Measurements of Total Attenuation, IEEE Transactions on Geoscience and Remote Sensing, GE-21, 34–43, doi:10.1109/TGRS.1983.350528, 1983.

Mie, G.: Beiträge zur Optik trüber Medien, speziell kolloidaler Metallösungen, Annalen der Physik, 330, 377–445, doi:10.1002/andp.19083300302, 1908.

Mishchenko, M. I., Travis, L. D., and Mackowski, D. W.: T-matrix computations of light scattering by nonspherical particles: A review, Journal of Quantitative Spectroscopy and Radiative Transfer, 55, 535–575, doi:10.1016/0022-4073(96)00002-7, 1996.

Moisseev, D. N. and Chandrasekar, V.: Examination of the μ–Λ Relation Suggested for Drop Size Distribution Parameters, Journal of Atmospheric and Oceanic Technology, 24, 847–855, doi:10.1175/JTECH2010.1, 2007.

Nelson, E. L., L'Ecuyer, T. S., Saleeby, S. M., Berg, W., Herbener, S. R., van den Heever, S. C., Nelson, E. L., L'Ecuyer, T. S., Saleeby, S. M., Berg, W., Herbener, S. R., and Heever, S. C. v. d.: Toward an Algorithm for Estimating Latent Heat Release in Warm Rain Systems, Journal of Atmospheric and Oceanic Technology, 33, 15–0205, doi:10.1175/JTECH-D-15-0205.1, 2016.

O'Connor, E. J., Hogan, R. J., and Illingworth, A. J.: Retrieving Stratocumulus Drizzle Parameters Using Doppler Radar and Lidar, Journal of Applied Meteorology, 44, 14–27, doi:10.1175/JAM-2181.1, 2005.

Rapp, A. D., Lebsock, M., L'Ecuyer, T., and L 'ecuyer, T.: Low cloud precipitation climatology in the southeastern Pacific marine stratocumulus region using CloudSat, Environmental Research Letters, 8, 014 027, doi:10.1088/1748-9326/8/1/014027, 2013.

Rodgers, C.: Inverse methods for atmospheric sounding: theory and practice, World Scientific, 2000.

Rose, C. R. and Chandrasekar, V.: A GPM Dual-Frequency Retrieval Algorithm: DSD Profile-Optimization Method, Journal of Atmospheric and Oceanic Technology, 23, 1372–1383, doi:10.1175/JTECH1921.1, 2006.

Stephens, G. L., Vane, D. G., Boain, R. J., Mace, G. G., Sassen, K., Wang, Z., Illingworth, A. J., O'Connor, E. J., Rossow, W. B., Durden, S. L., and others: The CloudSat mission and the A-Train, Bulletin of the American Meteorological Society, 83, 1771–1790, 2002.

Stephens, G. L., L'Ecuyer, T., Forbes, R., Gettlemen, A., Golaz, J.-C., Bodas-Salcedo, A., Suzuki, K., Gabriel, P., and Haynes, J.: Dreary state of precipitation in global models, Journal of Geophysical Research, 115, D24 211, doi:10.1029/2010JD014532, 2010.

Testud, J., Oury, S., Black, R. A., Amayenc, P., and Dou, X.: The Concept of "Normalized" Distribution to Describe Raindrop Spectra: A Tool for Cloud Physics and Cloud Remote Sensing, Journal of Applied Meteorology, 40, 1118–1140, doi:10.1175/1520-0450(2001)040<1118:TCONDT>2.0.CO;2, 2001.

Thurai, M., Huang, G. J., Bringi, V. N., Randeu, W. L., Schönhuber, M., Thurai, M., Huang, G. J., Bringi, V. N., Randeu, W. L., and Schönhuber, M.: Drop Shapes, Model Comparisons, and Calculations of Polarimetric Radar Parameters in Rain, Journal of Atmospheric and Oceanic Technology, 24, 1019–1032, doi:10.1175/JTECH2051.1, 2007.

Tian, L., Heymsfield, G. M., Li, L., and Srivastava, R. C.: Properties of light stratiform rain derived from 10- and 94-GHz airborne Doppler radars measurements, Journal of Geophysical Research, 112, D11 211, doi:10.1029/2006JD008144, 2007.

Tokay, A. and Short, D. A.: Evidence from Tropical Raindrop Spectra of the Origin of Rain from Stratiform versus Convective Clouds, Journal of Applied Meteorology, 35, 355–371, doi:10.1175/1520-0450(1996)035<0355:EFTRSO>2.0.CO;2, 1996.

Toon, O. B. O., Starr, D. O. D., Jensen, E. J., Newman, P. A., Platnick, S., Schoeberl, M. R., Wennberg, P. O., Wofsy, S. C., Kurylo, M. J., Maring, H., Jucks, K. W., Craig, M. S., Vasques, M. F., Pfister, L., Rosenlof, K. H., Selkirk, H. B., Colarco, P. R., Kawa, S. R., Mace, G. G., Minnis, P., and Pickering, K. E.: Planning, implementation, and first results of the Tropical Composition, Cloud and Climate Coupling Experiment (TC4), Journal of Geophysical Research, 115, D00J04, doi:10.1029/2009JD013073, 2010.

Twomey, S.: Introduction to the Mathematics of Inversion in Remote Sensing and Indirect, MeasuremenE Elsevier Scientific Publishing Co, 1977.

Weston, P. P., Bell, W., and Eyre, J. R.: Accounting for correlated error in the assimilation of high-resolution sounder data, Quarterly Journal of the Royal Meteorological Society, 140, 2420–2429, doi:10.1002/qj.2306, 2014.

Wilson, D. R., Illingworth, A. J., Blackman, T. M., Wilson, D. R., Illingworth, A. J., and Blackman, T. M.: Differential Doppler Velocity: A Radar Parameter for Characterizing Hydrometeor Size Distributions, Journal of Applied Meteorology, 36, 649–663, doi:10.1175/1520-0450-36.6.649, 1997.

Wood, R., Kubar, T. L., Hartmann, D. L., and Wood, R.: Understanding the Importance of Microphysics and Macrophysics for Warm Rain in Marine Low Clouds. Part II: Heuristic Models of Rain Formation, Journal of the Atmospheric Sciences, 66, 2953–2972, doi:10.1175/2009JAS3072.1, 2009.

Yoshida, R., Okamoto, H., Hagihara, Y., and Ishimoto, H.: Global analysis of cloud phase and ice crystal orientation from Cloud-Aerosol Lidar and Infrared Pathfinder Satellite Observation (CALIPSO) data using attenuated backscattering and depolarization ratio, Journal of Geophysical Research, 115, D00H32, doi:10.1029/2009JD012334, 2010.

Zhang, G., Vivekanandan, J., and Brandes, E.: A method for estimating rain rate and drop size distribution from polarimetric radar measurements, IEEE Transactions on Geoscience and Remote Sensing, 39, 830–841, doi:10.1109/36.917906, 2001.

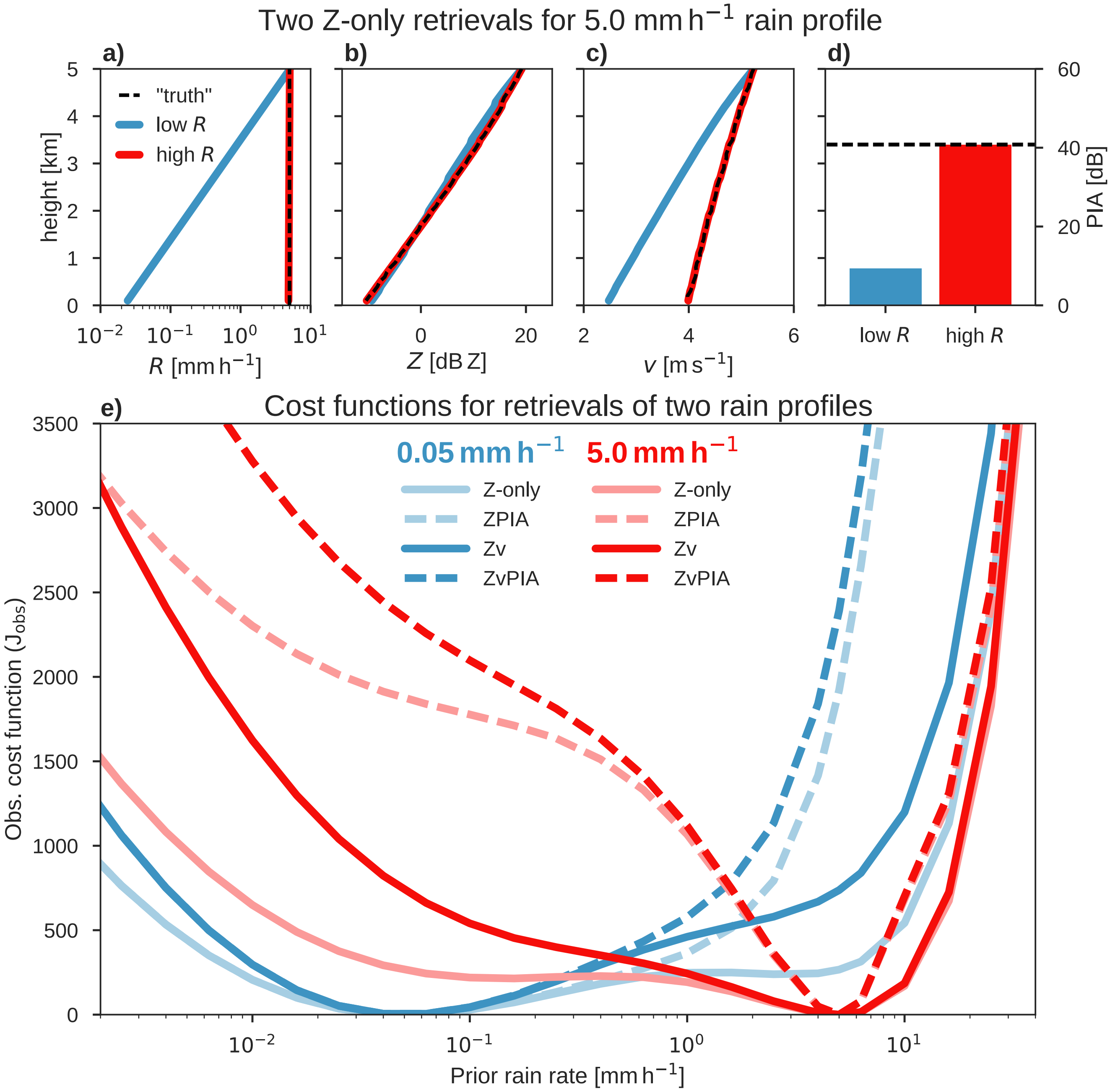

Figure 1. Above: Profiles of (a) retrieved rain rate, and (b) forward-modelled 94 GHz radar reflectivity, (c) mean Doppler velocity and (d) PIA, for the two solutions to the retrieval from a synthetic profile; dashed lines show the values corresponding to the "true" profile of constant $R = 5.0\,\mathrm{mm\,h^{-1}}$.

Below: (e) the observational component of the cost function (J_{obs}) for retrievals of two constant rain profiles with $R = 0.05\,\mathrm{mm\,h^{-1}}$ and $R = 5.0\,\mathrm{mm\,h^{-1}}$, initialised from a range of R priors. Bimodal or ambiguous retrievals are evident when using radar reflectivity alone (Z-only; light solid lines), and compared against retrievals using additional observational variables (Zv, ZPIA, and ZvPIA; dashed and dark lines) to resolve the ambiguity.

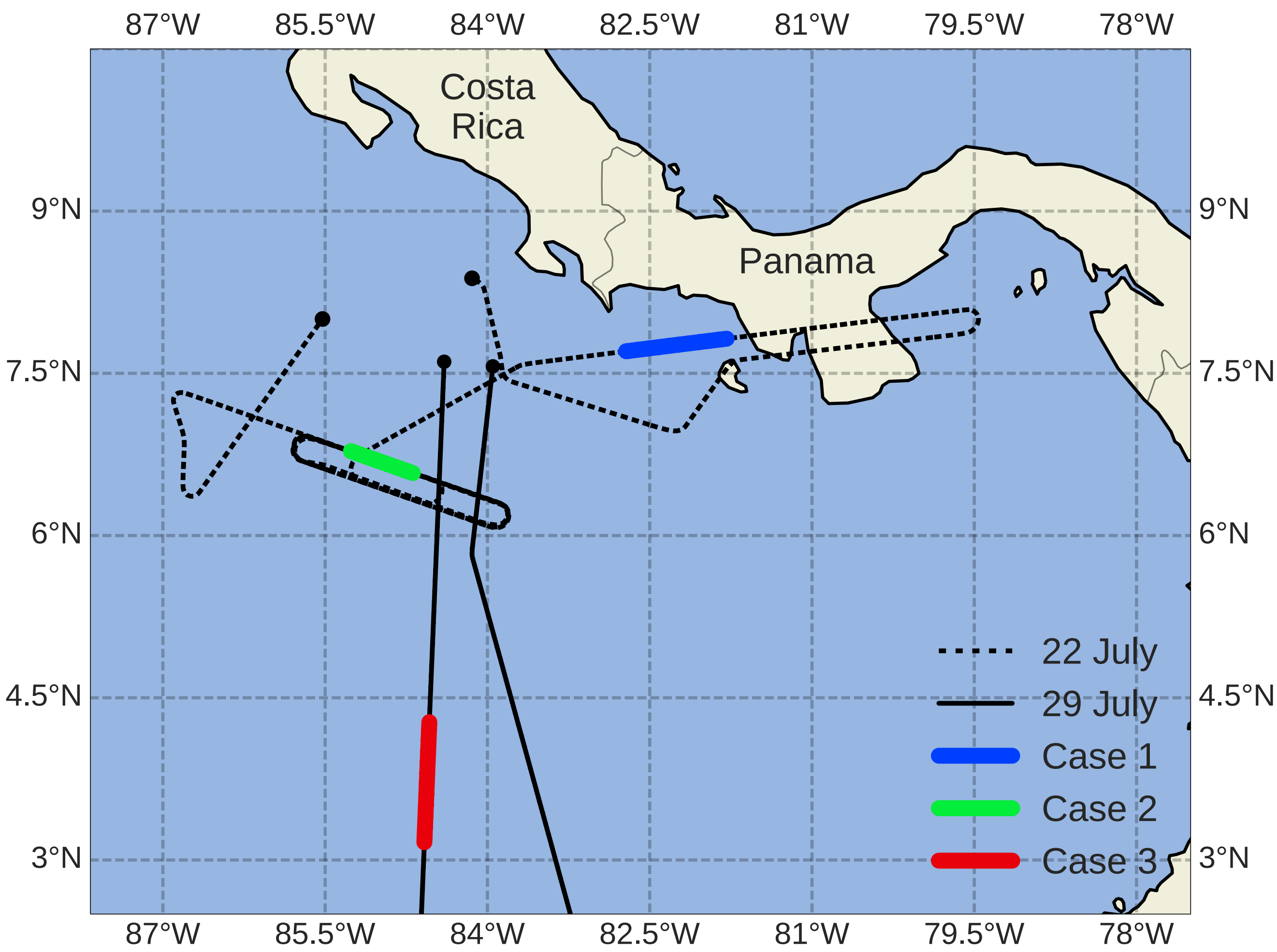

Figure 2. Flight tracks of the NASA ER-2 high-altitude aircraft over the tropical eastern Pacific on 22 July and 29 July 2007 during the TC4 field campaign. The flight legs selected for case studies of stratiform rain are highlighted.

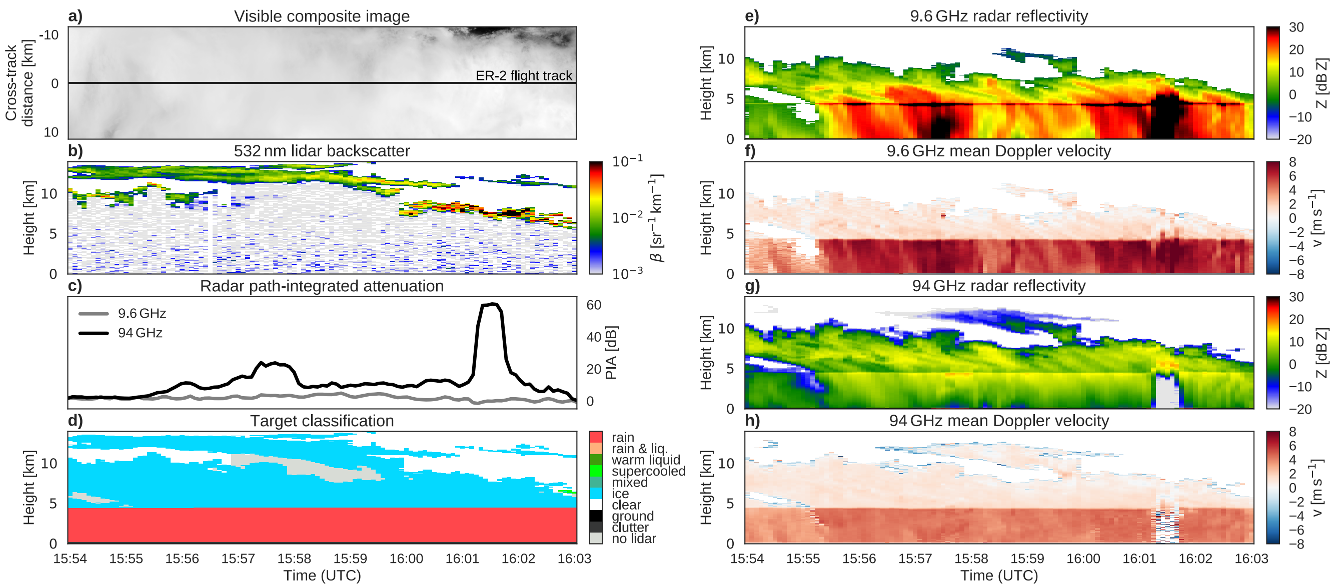

Figure 3. Selected measurements made by ER-2 instruments for Case 1 between 15:53 and 16:03 UTC on 22 July 2007 as part of TC4. Composite cloud scene (a) from MAS/MASTER visible channels, with the ER-2 flight track marked; 532 nm lidar backscatter (b); 9.6 and 94 GHz radar PIA (c); target classification from radar–lidar synergy (d); 9.6 GHz radar reflectivity (e) and mean Doppler velocity (f); and 94 GHz radar reflectivity (g) and mean Doppler velocity (h).

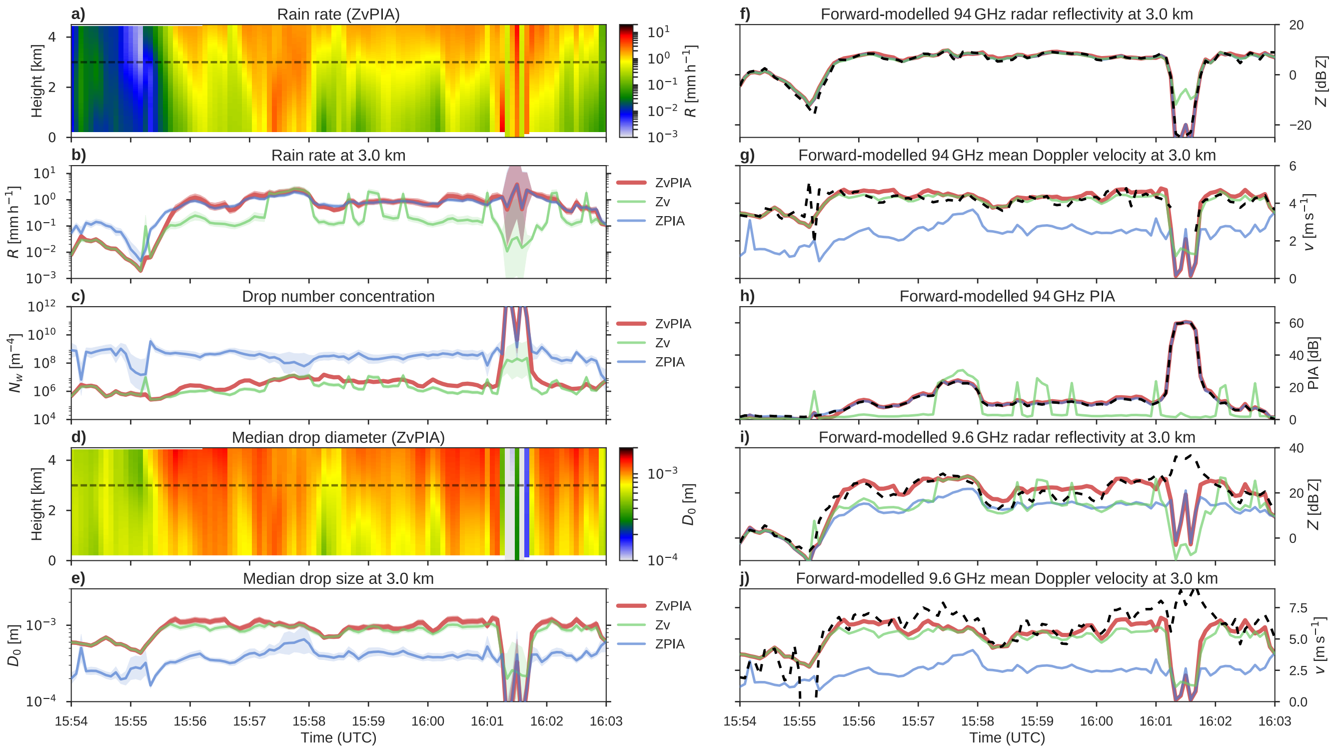

Figure 4. Time series of 94 GHz ZPIA, Zv and ZvPIA retrievals compared for Case 1 between 15:54 and 16:13 on 22 July 2007. Retrieved state and derived variables (left), and forward-modelled radar measurements (right) for the three retrievals are shown at a height of 3 km above sea level (indicated with a light dashed line in the left-hand scenes), while the full scenes of R (a) and D_0 (d) are shown for the ZvPIA retrieval. Shading indicates the 1-σ uncertainty in the retrieved and derived variables. Dark dashed lines (right) indicate the observed radar measurements.

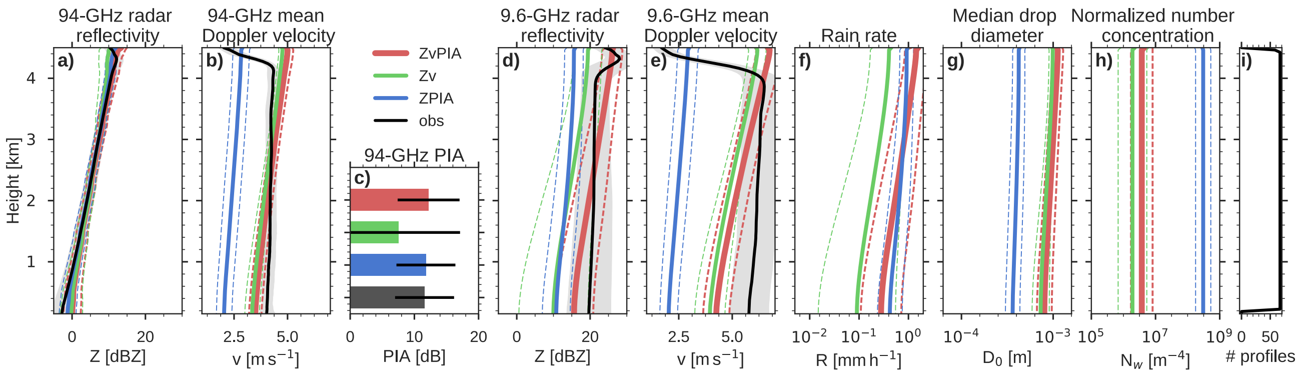

Figure 5. Averaged profiles of moderate rain between 15:55:30 and 16:11:00 UTC on 22 July 2007. Forward-modelled 94 GHz radar reflectivity (a), mean Doppler velocity (b) and PIA (c); forward-modelled 9.6 GHz radar reflectivity (d) and mean Doppler velocity (e); and retrieved rain rate (f), median drop size (g), number concentration parameter (h) for ZPIA, Zv and ZvPIA retrievals. The number of profiles included at each height is indicated in (i). Shading and dashed lines indicate the 1-σ uncertainty in the retrieved and derived variables.

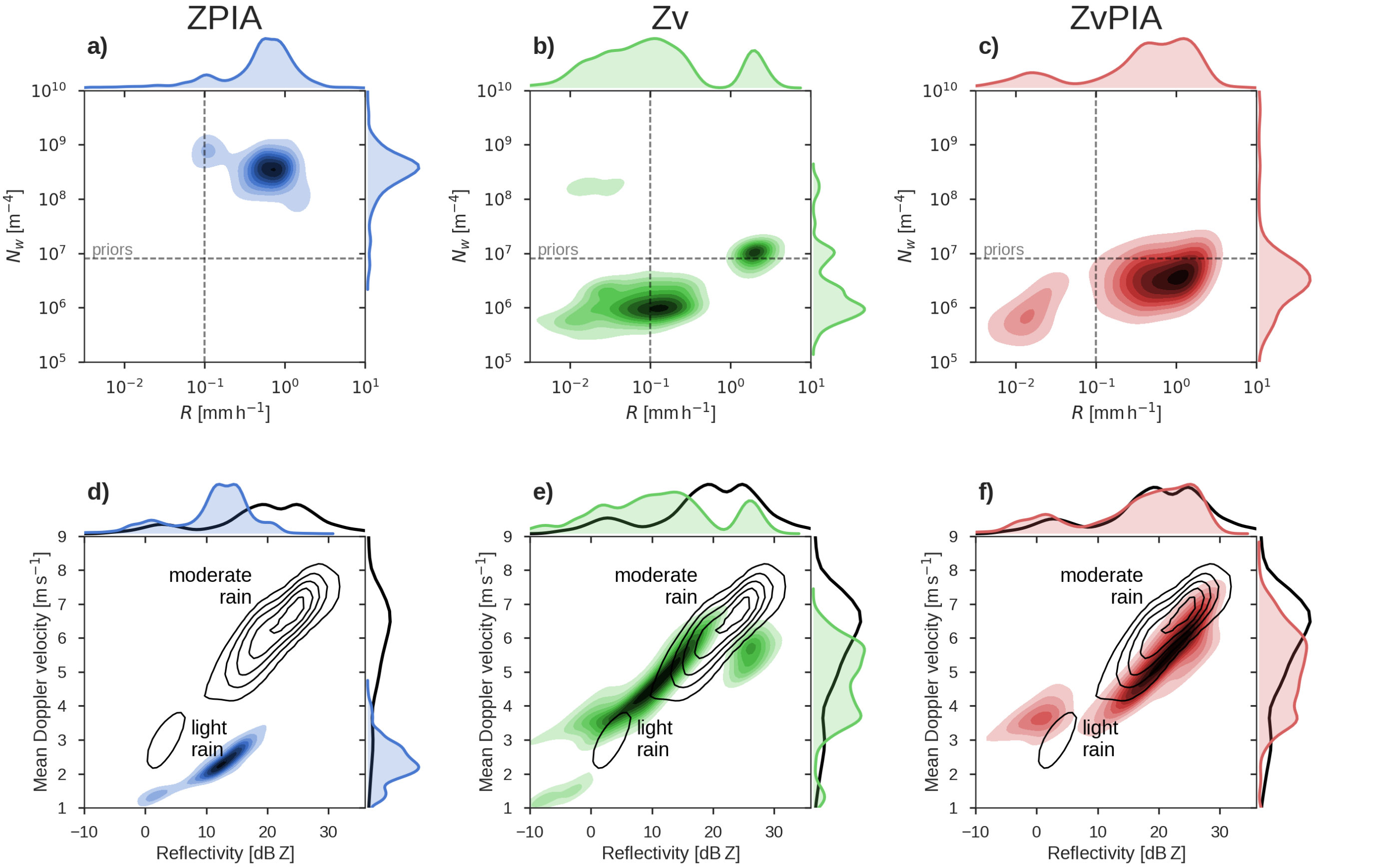

Figure 6. Joint (filled contours) and univariate (curves) kernel density estimation histograms of retrieved rain state variables R and N_w (a–c) and forward-modelled EDOP measurements (d–f) for ZPIA (a and d), Zv (b and e) and ZvPIA (c and f) rain retrievals during Case 1 on 22 July 2007. Dashed lines indicate the values of the prior state variables used in the retrieval. Black contours indicate the distribution of independent EDOP measurements; the major rain regimes are labelled.

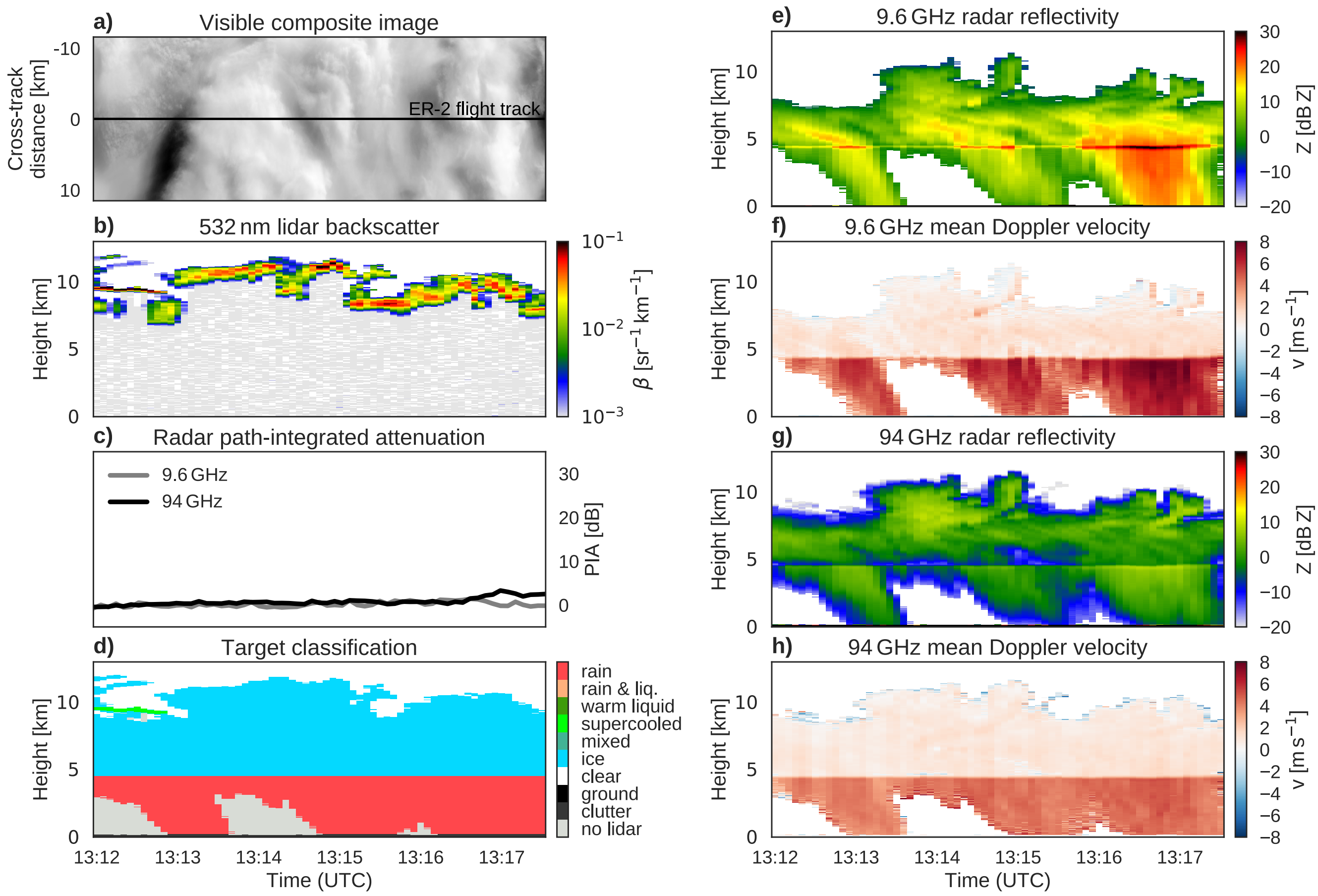

Figure 7. Selected measurements made by ER-2 instruments for Case 2 between 13:12:00 and 13:17:30 UTC on 22 July 2007 as part of TC4. The composite cloud image from MAS/MASTER visible channels (a), with the ER-2 flight track marked; 532 nm lidar backscatter (b); 9.6 and 94 GHz radar PIA (c); target classification from radar–lidar synergy (d); 9.6 GHz radar reflectivity (e) and mean Doppler velocity (f); and 94 GHz radar reflectivity (g) and mean Doppler velocity (h).

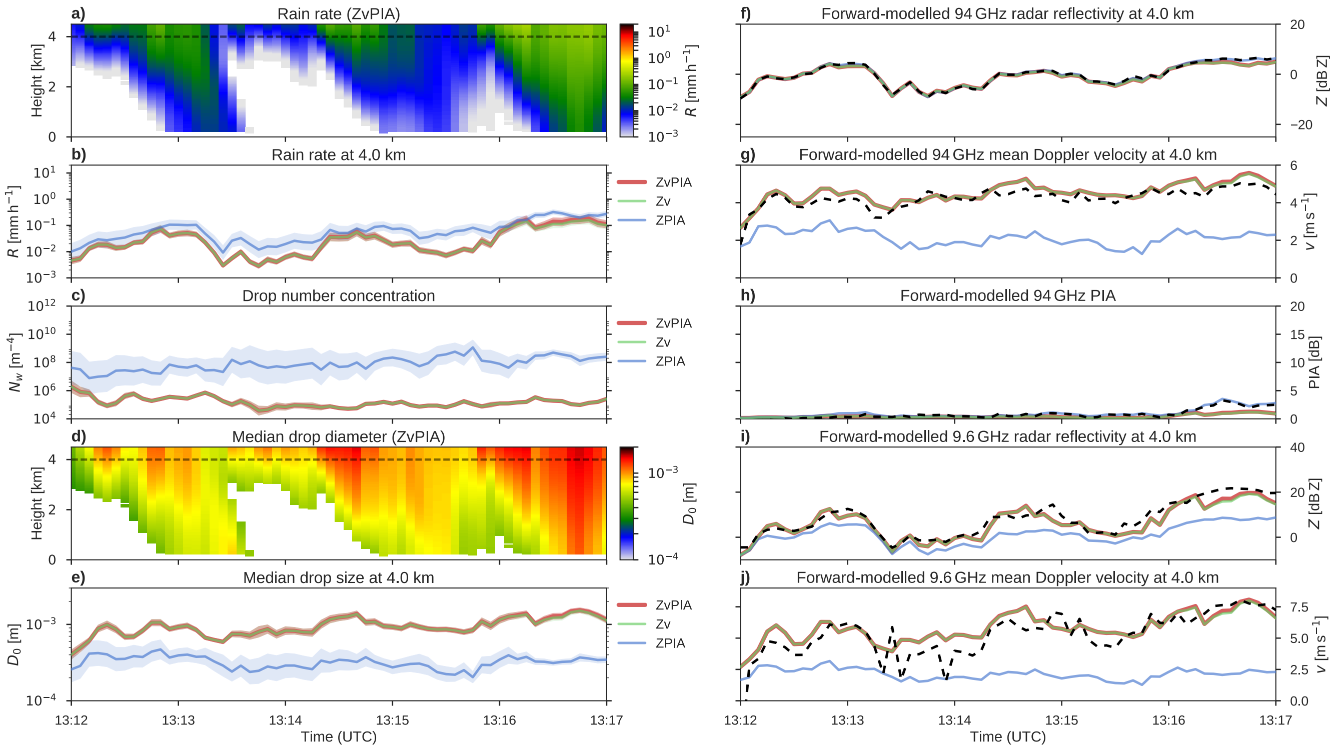

Figure 8. Time series of 94 GHz ZPIA, Zv and ZvPIA retrievals compared for Case 2 between 13:12 and 13:17 on 22 July 2007. Retrieved state and derived variables (left), and forward-modelled radar measurements (right) for the three retrievals are shown at a height of 4 km above sea level (indicated with a dashed line in the left-hand scenes), while the full scenes of R (a) and D_0 (d) are shown for the ZvPIA retrieval. In this case the observed PIA is negligible, so the ZvPIA retrieval has no more information than the Zv retrieval and the two lines are overlaid. Shading indicates the 1-σ uncertainty in the retrieved and derived variables. Black dashed lines indicate the observed radar measurements for comparison with the retrievals.

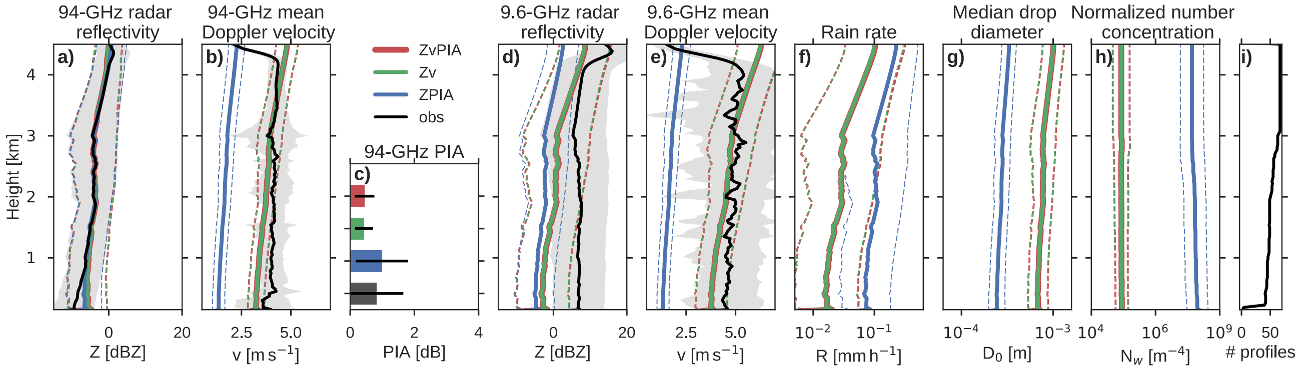

Figure 9. Averaged profiles of evaporating light rain between 13:12 and 13:17 on 22 July 2007. Forward-modelled 94 GHz radar reflectivity (a), mean Doppler velocity (b) and PIA (c); forward-modelled 10 GHz radar reflectivity (d) and mean Doppler velocity (e); and retrieved rain rate (f), median drop size (g), number concentration parameter (h) for ZPIA, Zv and ZvPIA retrievals. The number of profiles included at each height is indicated in (i). Shading and dashed lines indicate the 1-σ standard deviation of the retrieved and derived variables.

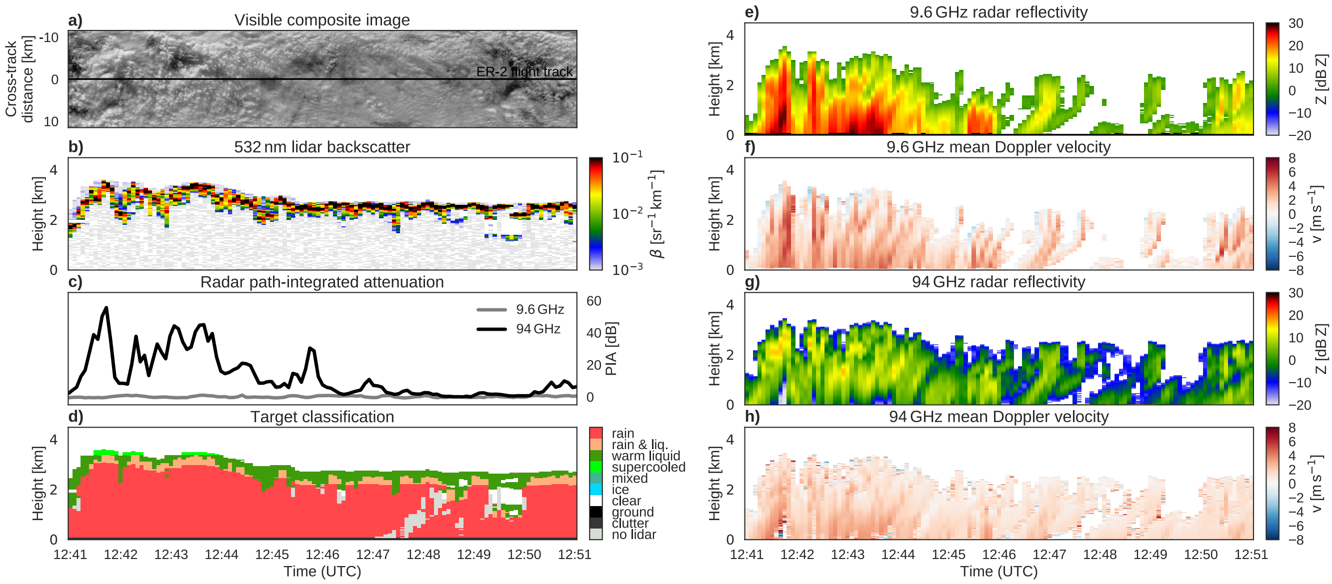

Figure 10. Selected measurements made by ER-2 instruments for Case 3 between 12:41 and 12:51 UTC on 29 July 2007 as part of TC4. Composite cloud scene (a) from MAS/MASTER visible channels, with the ER-2 flight track marked; 532 nm lidar backscatter (b); 9.6 and 94 GHz radar PIA (c); target classification from radar–lidar synergy (d); 9.6 GHz radar reflectivity (e) and mean Doppler velocity (f); and 94 GHz radar reflectivity (g) and mean Doppler velocity (h).

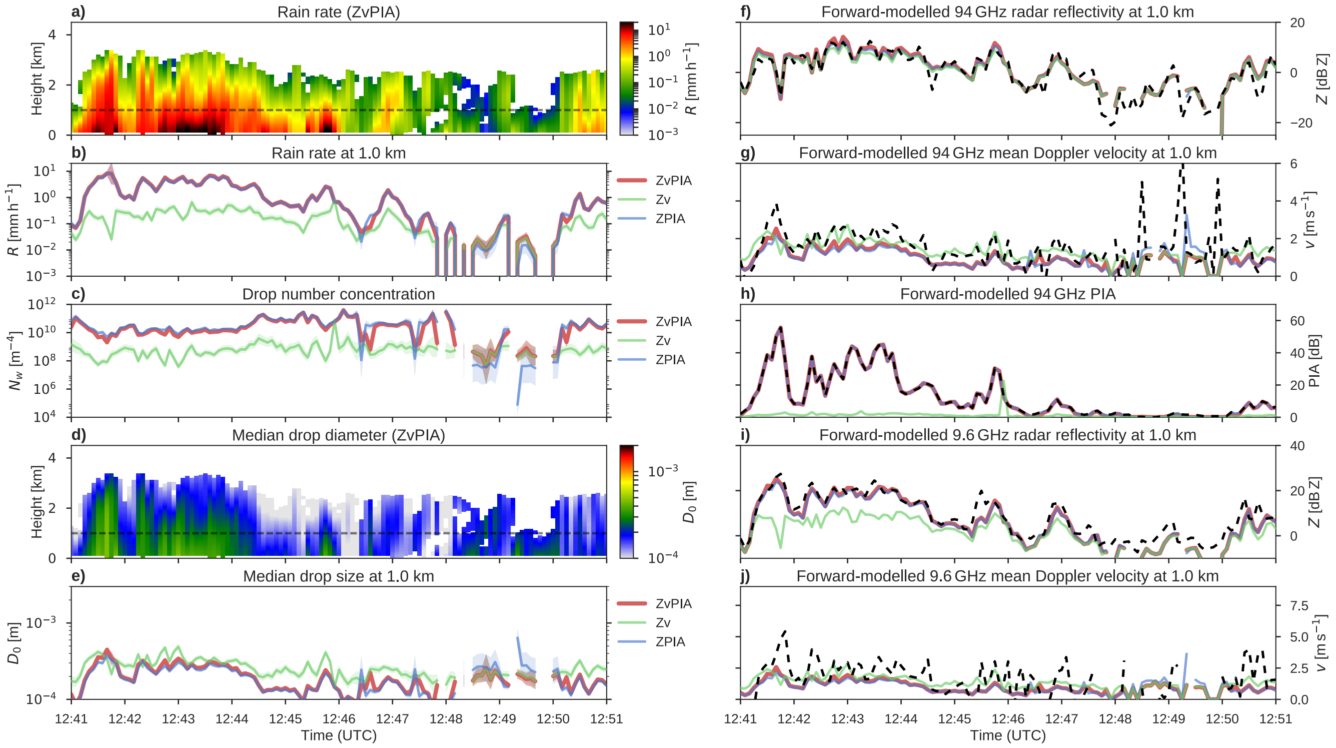

Figure 11. Time series of ZPIA, Zv and ZvPIA 94 GHz retrievals for Case 3 on 29 July 2007. Retrieved state and derived variables (left), and forward-modelled radar measurements (right) for the three retrievals are shown at a height of 1 km above sea level (indicated with a light dashed line in the left-hand scenes), while full scenes of R (a) and D_0 (d) are shown for the ZvPIA retrieval. Shading indicates the 1-σ uncertainty in the retrieved and derived variables. Dark dashed lines (right) indicate the observed radar measurements.

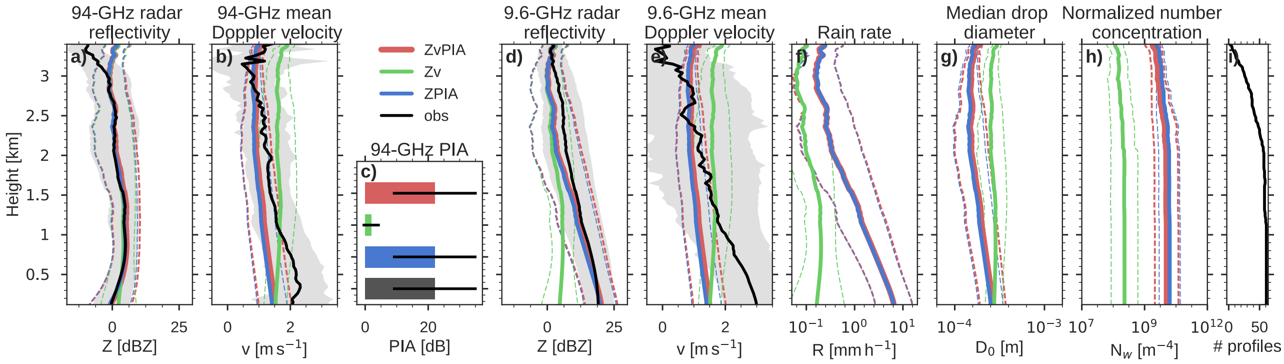

Figure 12. Averaged profiles of moderate rain between 12:41 and 12:46 UTC on 29 July 2007. Forward-modelled 94 GHz radar reflectivity (a), mean Doppler velocity (b) and PIA (c); forward-modelled 10 GHz radar reflectivity (d) and mean Doppler velocity (e); and retrieved rain rate (f), median drop size (g), number concentration parameter (h) for ZPIA, Zv and ZvPIA retrievals. The number of profiles included at each height is indicated in (i). Shading and dashed lines indicates the 1-σ standard deviation of the retrieved and derived variables.

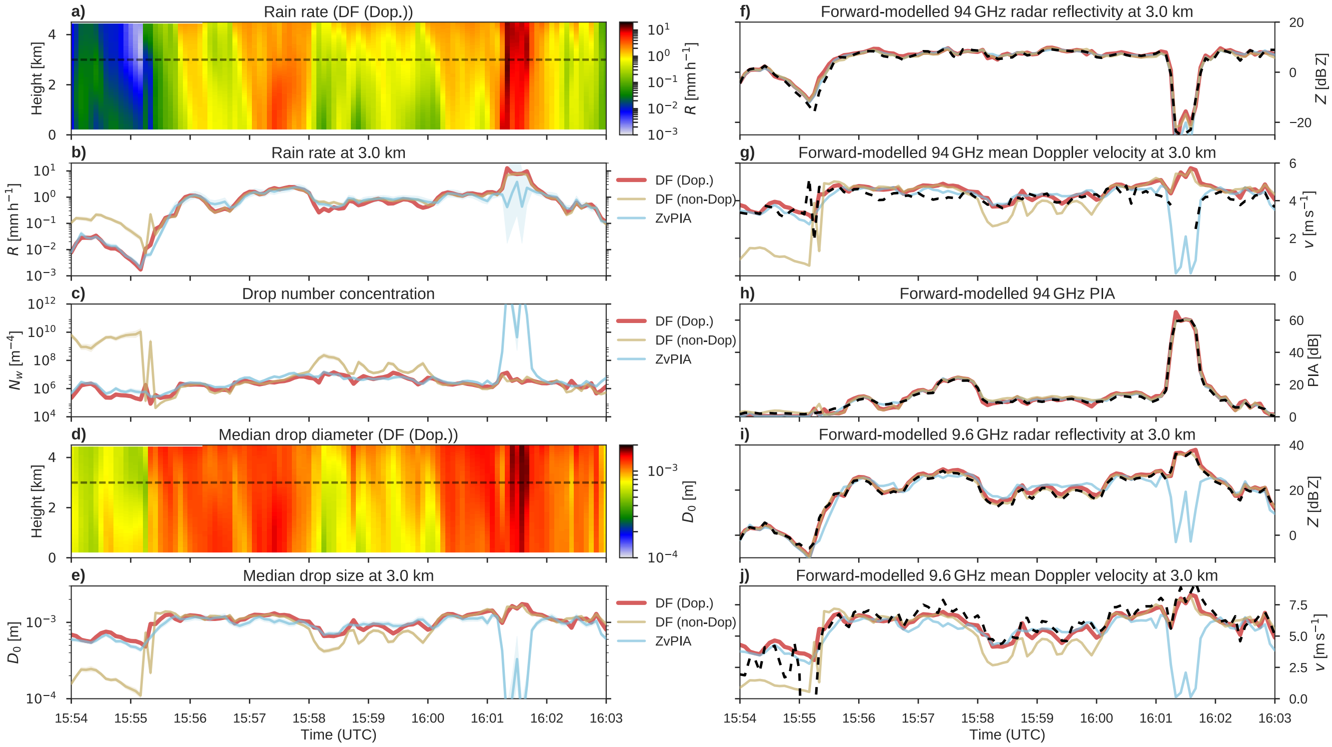

Figure 13. Time series of dual-frequency (DF) retrievals with and without Doppler, compared against the 94 GHz ZvPIA retrieval for Case 1 on 22 July 2007. Retrieved state and derived variables (left), and forward-modelled radar measurements (right) for the three retrievals are shown at a height of 3.0 km above sea level (indicated with a light dashed line in the left-hand scenes); while the full scenes of R (a) and D_0 (d) are shown for the dual-frequency Doppler retrieval. Shading indicates the 1-σ uncertainty in the retrieved and derived variables. Dark dashed lines (right) indicate the observed radar measurements.

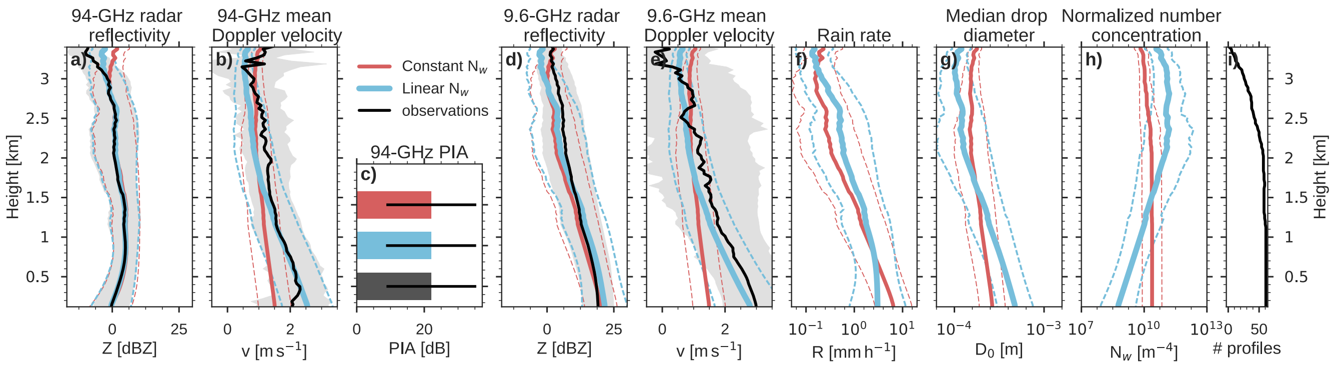

Figure 14. Averaged profiles of moderate rain between 12:41 and 12:46 UTC on 29 July 2007. Forward-modelled 94 GHz radar reflectivity (a), mean Doppler velocity (b) and PIA (c); forward-modelled 10 GHz radar reflectivity (d) and mean Doppler velocity (e); and retrieved rain rate (f), median drop size (g), drop number concentration parameter (h) for ZvPIA retrievals in which N_w is represented as a constant with height, and as a linear gradient. The number of profiles included at each height is indicated in (i). Shading and dashed lines indicate the 1-σ standard deviation of the retrieved and derived variables.